Development of Indian summer monsoon precipitation biases in two seasonal forecasting systems and their response to large-scale drivers

Richard J. Keane[1,2], Ankur Srivastava[3], Gill M. Martin[1]

[1]Met Office, Exeter, UK
5 [2]School of Earth and Environment, University of Leeds, UK
[3]Indian Institute of Tropical Meteorology, Ministry of Earth Sciences, Pune, India

Correspondence to: Richard J Keane (richard.keane@metoffice.gov.uk)

Abstract. The Met Office Global Coupled Model (GC) and the NCEP Climate Forecast System (CFSv2) are both widely used for predicting and simulating the Indian summer monsoon (ISM), and previous studies have demonstrated similarities in the

10 biases in both systems at a range of time scales from weather forecasting to climate simulation. In this study, ISM biases are studied in seasonal forecasting setups of the two systems, in order to provide insight into how they develop across time scales. Similarities are found in the development of the biases between the two systems, with an initial reduction in precipitation followed by a recovery associated with an increasingly cyclonic wind field to the north-east of India. However, this occurs on longer time scales in CFSv2, with a much stronger recovery followed by a second reduction associated with sea surface

15 temperature (SST) biases, so that the bias at longer lead times is of a similar magnitude to that in GC. In GC, the precipitation bias is almost fully developed within a lead time of just eight days, suggesting that carrying out simulations with short time integrations may be sufficient for obtaining substantial insight into the biases in much longer simulations. The relationship between the precipitation and SST biases in GC seems to be more complex than in CFSv2, and is different during the early part of the monsoon season from during the later part of the monsoon season.

20 The relationship of the bias with large-scale drivers is also investigated, using the Boreal Summer IntraSeasonal Oscillation (BSISO) index as a measure of whether the large-scale dynamics favours increasing, active, decreasing or break monsoon conditions. Both models simulate decreasing conditions the best and increasing conditions the worst, in agreement with previous studies and extending these previous results to include CFSv2 and multiple BSISO cycles.

Copyright statement

1 Introduction

30   The Indian summer monsoon (ISM) is one of the most challenging meteorological phenomena to simulate, with many current general circulation models (GCMs) having substantial systematic biases (Jain et al., 2019; Katzenberger et al., 2021; Mitra, 2021; Watterson et al., 2021; Choudhury et al, 2022). Two examples of GCMs with a persistent low-precipitation bias for the ISM are the Met Office Global Coupled Model (GC, Williams et al., 2015; 2017) and the NCEP Climate Forecast System (CFSv2, Saha et al., 2014). This has been shown to occur in these models across a range of time scales—with common

35   accompanying features including an anti-cyclonic bias and a high-precipitation bias over the ocean to the south of India—from weather forecasts (Kar et al., 2019; Keane et al., 2019; 2021; Abhilash et al., 2014) to seasonal and climate simulations (Walters et al., 2019; Martin et al., 2021; Swapna et al., 2018; Sahana et al, 2019). The purpose of the present study is to investigate this low-precipitation bias in detail in seasonal simulations, to provide insight into how it develops from shorter to longer time scales.

40   Many previous studies have investigated the skill of seasonal forecasts, using GC or CFSv2, in predicting the ISM, and these studies have generally demonstrated similar biases to those in weather and climate simulations (Abhilash et al., 2014; George et al., 2016; Ramu et al., 2016; Johnson et al., 2017; Srivastava et al., 2017; Jain et al., 2019; Chevuturi et al., 2019; Martin et al., 2021; Joseph et al., 2023; Kolusu et al., 2023). Despite these biases, the seasonal forecasts do show skill, particularly at shorter lead times (George et al., 2016; Rao et al., 2019; Joseph et al., 2023; Kolusu et al., 2023) and can reasonably well

45   simulate the northward propagation of the monsoon intraseasonal oscillation (Abhilash et al., 2014; Sabeerali et al., 2013; Srivastava et al., 2023), low-pressure systems (Srivastava et al., 2017; 2023) and the monsoon onset (Menon et al., 2018; Chevuturi et al., 2019; Pradhan et al. 2017). George et al. (2016) attributed this skill in CFSv2 to correctly capturing connections with the El Nino Southern Oscillation, with Indian Ocean coupled dynamics not adequately represented in CFSv2, and similar behaviour was demonstrated for GC by Johnson et al. (2017).

50   The atmospheric biases have been shown to be associated with cold sea-surface temperature (SST) biases in CFSv2 (George et al., 2016; Srivastava et al., 2017) and GC has also been shown to develop SST biases in seasonal forecasts within the first 30 days (Martin et al., 2021); Johnson et al. (2017) attributed incorrect SST anomalies to a lack of wind forcing on the SSTs. We investigate this interdependence of atmospheric and oceanic biases in the seasonal forecasting systems here by carrying out a systematic investigation of the variation of how precipitation, wind and SST biases vary with forecast lead time.

55   Martin et al. (2021) investigated systematic biases for the Asian summer monsoon, in GC configurations on a range of time scales. They showed that, while the biases in seasonal forecasts and climate simulations generally have similar patterns and magnitudes, those over India have larger magnitudes in the climate simulations, indicating that these biases could have a substantial dependence on how far ahead of the monsoon season the simulation is initialised. Meanwhile, Chattopadhyay et al. (2016) demonstrated an intriguing finding that, in CFSv2, longer lead times can produce better ISM forecasts than shorter lead

60   times. It is therefore important to look at the lead-time development of the seasonal forecast biases in detail to investigate how they are affected by errors in different physical processes occurring on different time scales.

A more direct aim of this study is to follow Keane et al. (2021), who showed that the reduction in mean ISM precipitation with forecast lead time in weather forecasts using the atmosphere and land components of GC has a strong and coherent dependence on the phase of the Boreal Summer Intraseasonal Oscillation (BSISO; Wang & Xie, 1997; Kikuchi et al., 2012; Lee et al.,
65 2013; Kikuchi, 2020; Kikuchi, 2021). They showed that the precipitation is initially too high for all phases, and the subsequent reduction is strongest for phases 2–4, corresponding to broadly increasing monsoon activity, so that by the end of the forecast there is a substantial low-precipitation bias. For phases 5–7, corresponding to broadly decreasing monsoon activity, the reduction is much weaker so that the value at the end of the forecast is actually quite close to observed values. It is therefore of interest to investigate longer forecasts with the same model to investigate how this behaviour develops beyond the 7 days
70 of the weather forecasts, as well as the influence of ocean-atmosphere coupling. This study provides an opportunity to do this, as well as to determine whether a similar dependence of the precipitation bias with BSISO phase occurs in CFSv2.

The manuscript proceeds by describing the data evaluated in this study and the methods used to perform the evaluation. The results of the evaluation are then presented, followed by a summary and concluding remarks.

2 Data

75 The GC setup for producing seasonal forecasts is GloSea, described in detail by MacLachlan et al. (2015). The forecasts are calibrated by running a set of hindcasts initialised at the same time of year as the forecast for a range of previous years using the same model version, so that the model version's statistical errors relative to the relevant seasonal climatology can be determined. The hindcasts are initialised as a 7-member ensemble on the 1st, 9th, 17th and 25th of each month for the year range 1993–2016. The hindcasts are therefore used in this study as they provide a large data set and we are interested in the
80 development of biases in the dynamical model itself rather than the quality of the post-processed forecasts.

Operational upgrades to GloSea have always been carried out less often than once per year, meaning that there is at least one full year's worth of hindcasts available for each version. In this study we assess two versions, GloSea5 based on GC2.0 (Williams et al., 2015), using hindcasts generated during the period from November 2017 to August 2018, and GloSea6 based on GC3.2 (closely related to GC3.0 and GC3.1, described by Williams et al., 2017), using hindcasts generated during the
85 period from November 2021 to August 2022. The atmospheric model resolution of both GloSea versions is N216, corresponding to grid spacings of approximately 70 km in the tropics. ERA-interim reanalysis fields are used to provide the (unperturbed) initial conditions and perturbations between the members are produced through the use of a stochastic kinetic energy backscatter scheme (Bowler et al., 2009). An upgrade to the soil moisture initialisation (described by Gautam et al., 2023) was implemented in 2019 so GloSea6 includes this upgrade whereas the version of GloSea5 evaluated here does not.
90 Hindcasts have also been produced using CFSv2. The atmospheric model spectral resolution is T382, corresponding to grid spacings of approximately 38 km in the tropics. Two hindcasts were initialised, at 00UTC and 12UTC, roughly every 5 days from February to August for the year range 2002–2015; the precise initialisation dates are provided in Table A1. This means that there are roughly half as many hindcasts initialised during the period February–August each year for CFSv2 (74) as for

GloSea (196), but we compare the two systems directly in the main manuscript and show evidence in Appendix A that using
95   only three of the seven GloSea ensemble members (so giving 84 hindcasts initialised during February–August) does not affect
the key conclusions of the paper (Figs. A1, A9). We restrict our evaluation to the period 2002–2015 but, again, show evidence
in Appendix A that these years are representative of the full period for which GloSea hindcasts are available (Figs. A2, A10).
In this study we evaluate the behaviour of the hindcasts as a function of lead time for given valid time periods. To do this, for
each lead time we average the hindcast values over all initialisation dates with a hindcast of the corresponding length occurring
100   during the relevant valid time period. We focus on valid times during June–August, and the total hindcast length is 216 days
for GloSea and 208 days for CFSv2. This means that the earliest GloSea hindcasts used are initialised on 1st November the
previous year, where the longest lead times extend just into the beginning of June, and the number of available hindcasts for
every lead time is approximately the same (12 or 13). However, since the CFSv2 hindcasts are only available from February,
hindcasts at the longest lead times are only available later in the June–August period (for example, lead times longer than 150
105   days are only available for July and August valid times).

We also carry out some evaluation of the hindcasts by taking all those initialised during a certain period and categorising them
according to the BSISO state at the start of the hindcast. We look at how the precipitation varies as the hindcast develops, up
to a hindcast time of 60 days, averaged over all hindcasts within each category, and compare with the observed precipitation
averaged over the corresponding dates.

110   The purpose of this study is to investigate how model quantities change as the hindcast develops (whether looking at a given
set of valid times and increasing the lead time by looking at different hindcasts, or looking at a given set of initialisation times
and increasing the integration times of the same hindcasts), rather than to evaluate their performance with respect to
observations, which is generally already well known at least in the broadest sense. However, we do compare with observed
precipitation, using the IMERG data set (Huffman et al., 2019), in order to provide a baseline for the modelled quantities.

115   In this study, observed BSISO data are taken from https://iprc.soest.hawaii.edu/users/kazuyosh/ISO_index/data/BSISO_25-
90bpfil_pc.extension.txt. The BSISO index is calculated using temporally bandpass filtered observed outgoing longwave
radiation (OLR). An extended empirical orthogonal function (EEOF) analysis is carried out on the data for June–October, and
for any given day, principal components can be obtained by projecting the OLR field onto each EEOF. The first two principal
components are normalised and can then be plotted on orthogonal axes. A phase and amplitude can then be defined as the
120   azimuthal and radial coordinate of the plotted point on the orthogonal axes. The full method is described by Kikuchi et al.
(2012) and Kikuchi (2020).

In practice, the azimuthal coordinate is divided into eight discrete phases, with phases 4 & 5 generally corresponding to
increased average precipitation over India and phases 8 & 1 corresponding to reduced average precipitation over India (Kikuchi
et al., 2012). We therefore use the phases as an indicator of whether the large-scale dynamics favours enhanced, increasing,
125   suppressed or decreasing convection over India and categorise the hindcasts using two different methods, one using the phase
at the hindcast valid time and one using the phase at the hindcast initialisation time, as described above.

3 Results

3.1 General Behaviour

The precipitation averaged over latitudes 8N–29N and longitudes 69E–89E, and over valid times during June–August 2002–
130   2015, is shown for each hindcast lead time in Fig. 1. This is the region investigated in detail by Keane et al. (2021) and is used
in this study when looking at spatially averaged quantities. Versions of Fig. 1 using fewer GloSea members and using a longer
range of GloSea years are shown in Appendix A (Figs. A1 and A2, respectively), and are very similar. Because hindcasts are
only initialised on certain dates within each system, hindcasts at a given lead time will only be available on a subset of the 92
days during June–August each year. For example, in GloSea, at 10 days' lead time there are hindcasts available on 4th, 11th,
135   19th, 27th June, 5th, 11th, 19th, 27th July, and 4th, 11th, 19th, 27th August; at most lead times there are 12 hindcasts available, with
13 available at some lead times due to the slight irregularity in the rate of initialisation of the hindcasts. The rate of initialisation
for the CFSv2 hindcasts is slightly more irregular, so that there are 15—18 dates available for each lead time up to 137 days
(after which the number of available dates gradually decreases, as described in the previous section). The dotted lines therefore
show the observed precipitation on the same subsets of dates, and provide an estimate of how much this variation in available
140   dates with lead time should affect the hindcast.

Looking at Fig. 1, CFSv2 and GloSea5 reach a similar low-precipitation bias by the end of the hindcast, but this takes longer
to develop in CFSv2. GloSea6 also has a low-precipitation bias but this is much improved compared with GloSea5. Both
GloSea systems have increasing precipitation at very short lead times and then all systems have sharply decreasing precipitation
during the first 8 days or so. The development is then characterised by a slower decrease followed by a recovery, but this is
145   much stronger, and takes longer to develop, in CFSv2 and is very weak in GloSea6. In CFSv2 there is then a decrease followed
by fairly constant values from about 100 days, while in GloSea the precipitation is fairly constant from about 30 days.
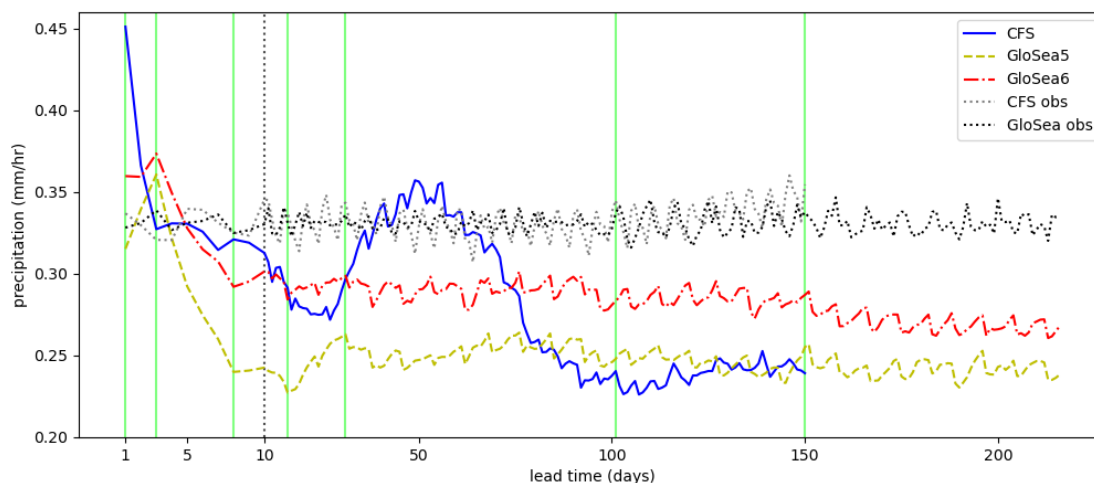
Figure 1: Variation of precipitation (averaged over 8N–29N and 69E–89E and June–August 2012–2015) with hindcast lead time in different seasonal forecasting systems. The dotted lines show observed values averaged over the dates on which hindcasts were available in the specified system at that lead time. The green vertical lines show the lead times used in Figs. 2–7 (1, 3, 8, 16, 31, 50, 101 and 150 days). Note that the horizontal scale is larger for lead times less than 10 days than for lead times greater than 10 days (so that it is different either side of the vertical dotted grey line).

3.2 Changes during specific stages of the hindcast

In order to investigate the behaviour in more detail, the hindcasts are divided into different stages, following the evolution shown in Fig. 1. The first two days are characterised by increasing precipitation in GloSea and decreasing precipitation in CFSv2. In GloSea this may be due to a 'spin-up' from the reanalysis initial state toward behaviour more representative of GC. The next five days account for most of the low-precipitation bias in both GloSea setups. The following eight days have fairly constant precipitation in GloSea and decreasing precipitation in CFSv2, while the next fifteen days after that have a small increase in precipitation in GloSea and fairly constant values in CFSv2. The subsequent period of approximately nineteen days has increasing precipitation in CFSv2, then there is a period of approximately fifty days of decreasing precipitation in CFSv2. These two periods have fairly constant precipitation in GloSea and the period from 100 days onwards has fairly constant precipitation in all setups.

To investigate this further, maps of precipitation, 850-hPa wind and SST, in the form of differences between pairs of lead times corresponding to the green vertical lines in Fig. 1, are plotted in Figs. 2–7. The absolute values are plotted in Figs. A3–A8 and are characterised by a prevailing westerly flow over India and widespread precipitation, with the largest amounts on the west coast and north-east of India and the Bay of Bengal (BoB).
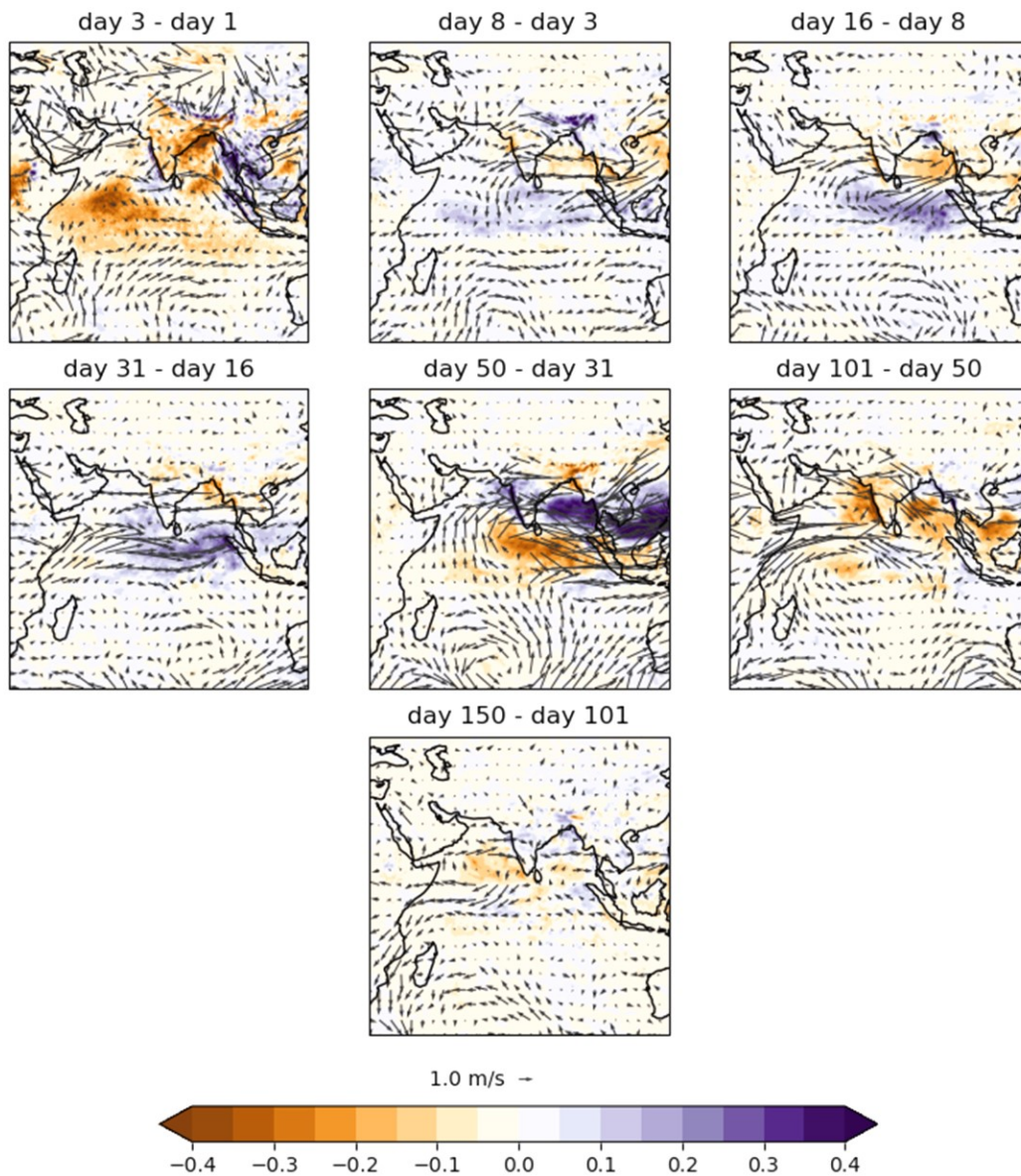
Figure 2: Precipitation differences (colours, in mm/hr) and 850-hPa wind differences (vectors) in CFSv2, between the hindcast lead times shown, averaged over June–August 2012–2015.

170
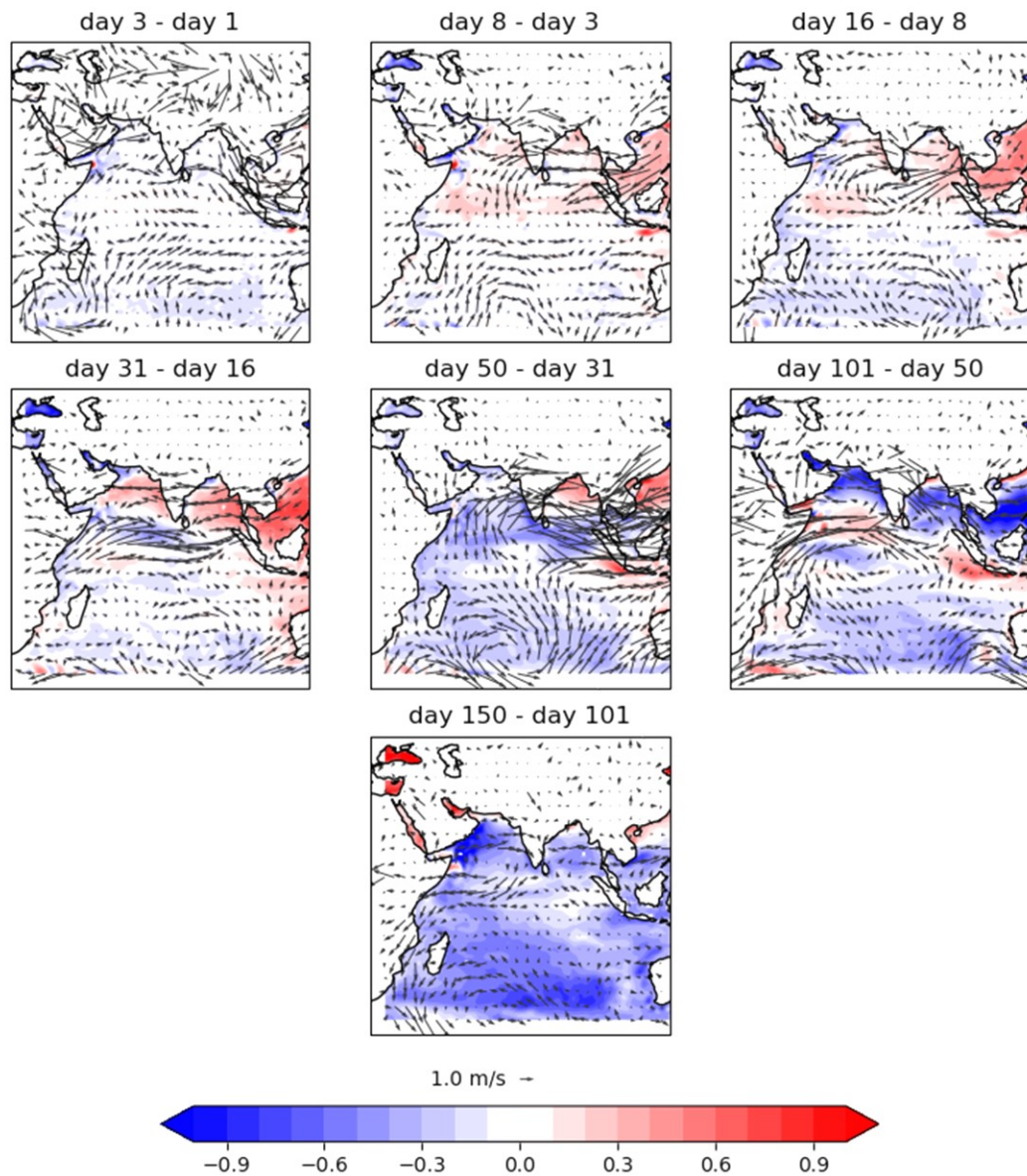
Figure 3: SST differences (colours, in K) and 850-hPa wind differences (vectors; note that this field is identical to that in Fig. 2) in CFSv2, between the hindcast lead times shown, averaged over June–August 2012–2015.
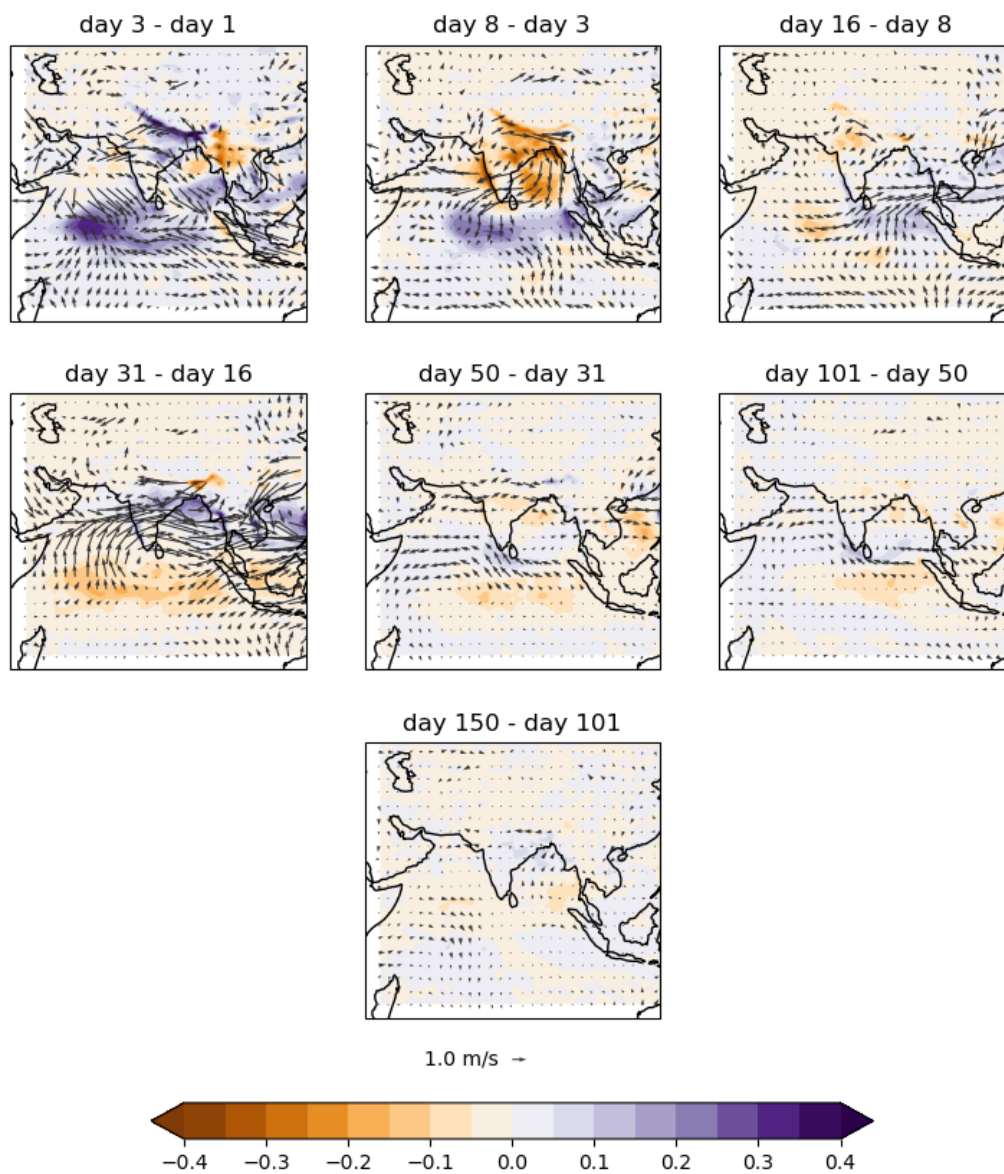
Figure 4: Precipitation differences (colours, in mm/hr) and 850-hPa wind differences (vectors) in GloSea5, between the hindcast lead times shown, averaged over June–August 2012–2015.

175
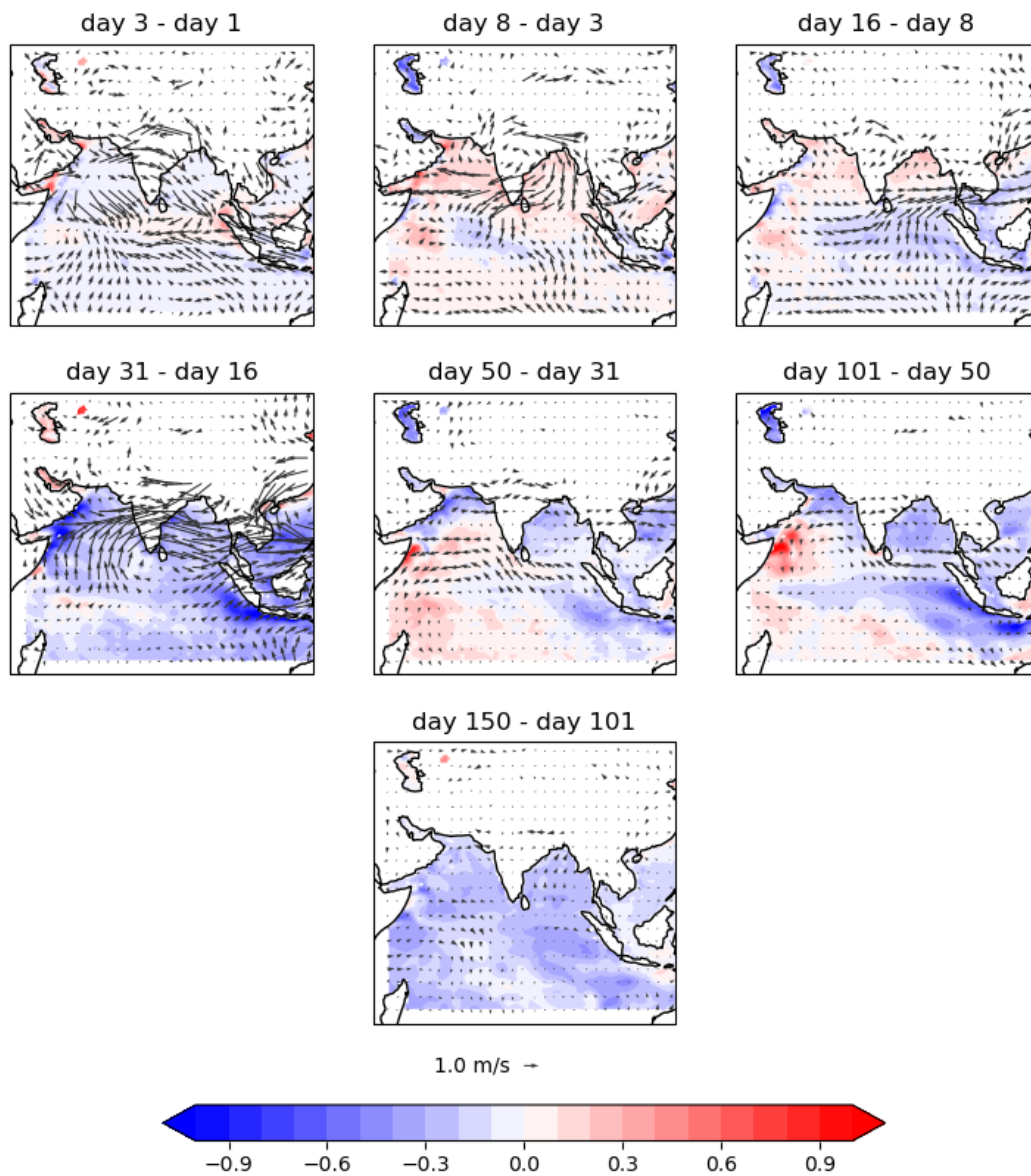
Figure 5: SST differences (colours, in K) and 850-hPa wind differences (vectors; note that this field is identical to that in Fig. 4) in GloSea5, between the hindcast lead times shown, averaged over June–August 2012–2015.
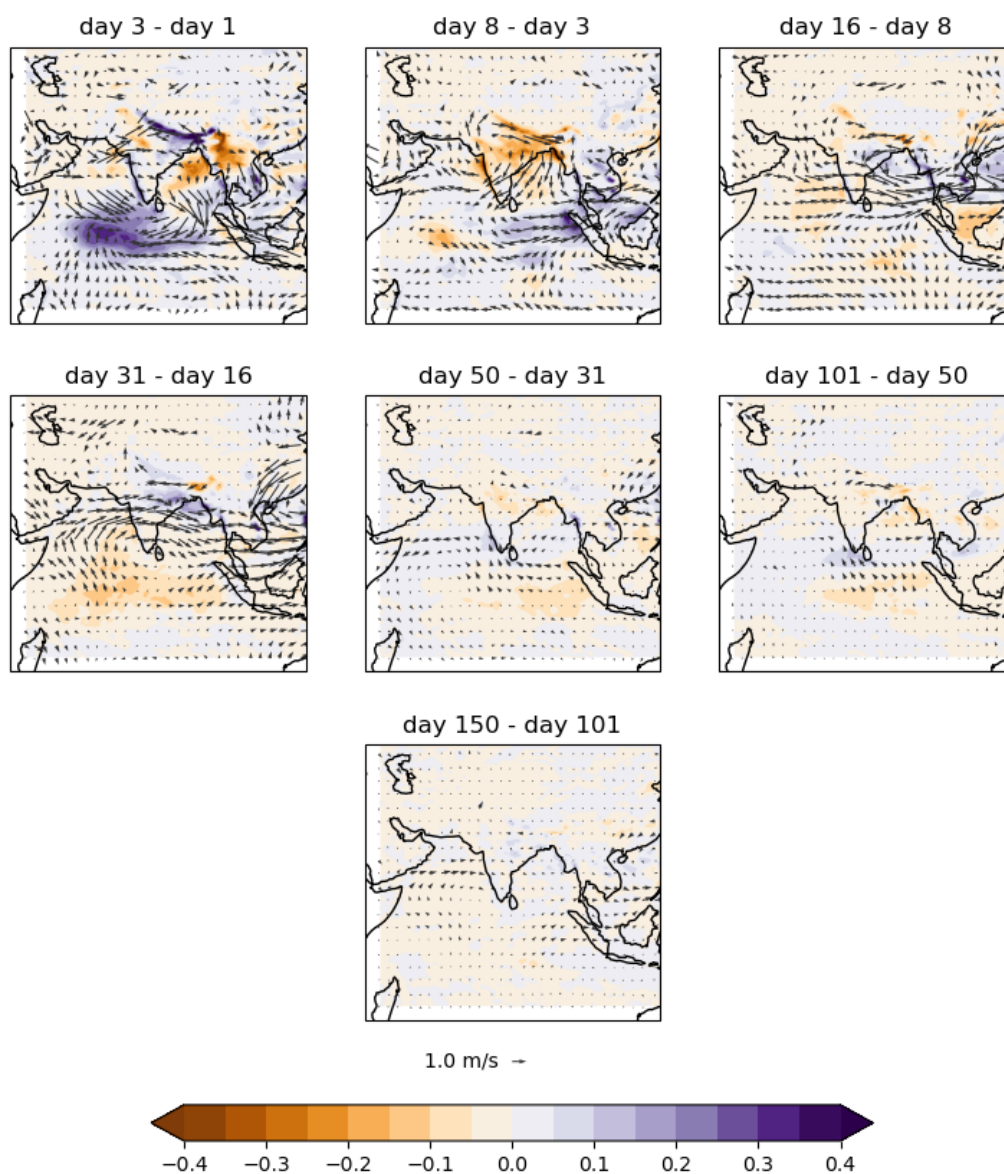
Figure 6: Precipitation differences (colours, in mm/hr) and 850-hPa wind differences (vectors) in GloSea6, between the hindcast lead times shown, averaged over June–August 2012–2015.
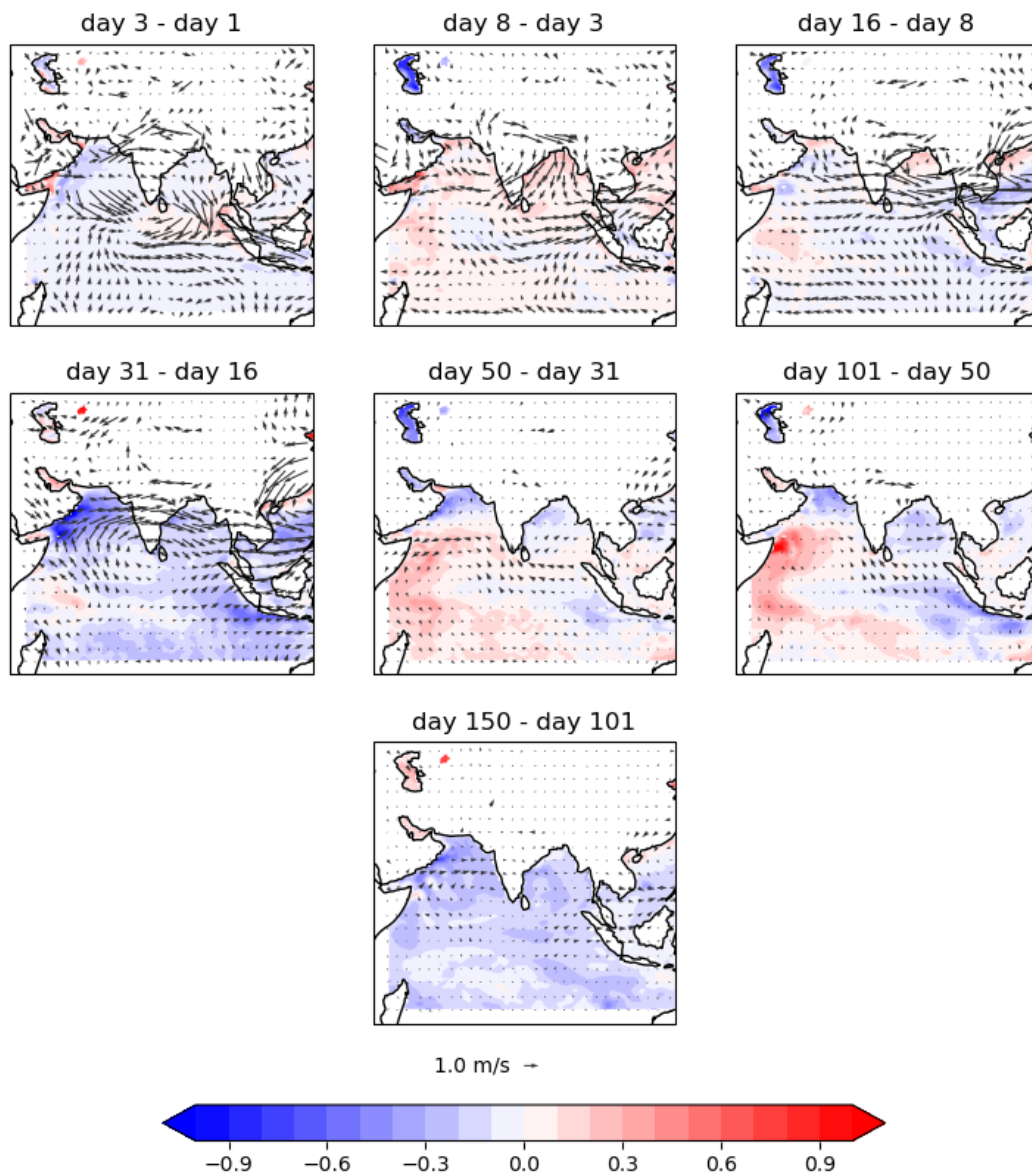
Figure 7: SST differences (colours, in K) and 850-hPa wind differences (vectors; note that this field is identical to that in Fig. 6) in GloSea6, between the hindcast lead times shown, averaged over June–August 2012–2015.

185

During days 1 to 3, the overall westerly flow strengthens in all three systems (albeit rather less coherently in CFSv2), but diverges away from India, in that it is too southerly in the north and too northerly in the south. In GloSea this is accompanied by an increase in precipitation over India and the Equatorial Indian Ocean (EIO), whereas in CFSv2 there is a sharp decrease. There is also increased convergence into the EIO in GloSea. This time period is generally too short for any SST changes to

190   develop.

During days 3 to 8, most of the precipitation reduction occurs in GloSea and it is accompanied by an anticyclonic bias, as seen in previous studies of GC) on weather and climate time scales. The precipitation bias is considerably reduced in GloSea6 but the anticyclonic bias is similar to that in GloSea5. The behaviour is similar in CFSv2 but with rather less coherent patterns. All systems show a decrease in the westerly flow into the south of India, although this is less pronounced in GloSea6. The

195   behaviour during the first 8 days in GloSea is consistent with that in the atmosphere-only weather forecasts studied by Keane et al. (2019; 2021).

Days 8 to 16 represent a relatively quiet period for GloSea in terms of precipitation, but v5 has an increase in anticyclonic flow whereas v6 becomes more cyclonic and the westerly flow into India increases, mitigating the bias in the previous period. CFSv2 also has small precipitation changes over India but there is a decrease over the BoB and an increase over EIO. The

200   flow also becomes more anticyclonic to the east of India. The reduction in precipitation over the BoB is accompanied by an increase in SST and a reduction in the flow from India. SST changes are still very small in GloSea, but with some notable increase over the EIO.

Days 16 to 31 show an increase in the westerly flow In GloSea, bringing increased precipitation over the western coast, and an increase in cyclonic flow, bringing increased precipitation to the very east of India and northern BoB. These features are

205   more pronounced in v5, which could be related to the fact that the reduction in precipitation during earlier periods is stronger, and so there is more scope for a recovery in precipitation. CFSv2 looks very different, with decreased westerly flow over India and reduced precipitation over the northern BoB. The flow to the south of India is more westerly, with (as in the previous period) an increase in precipitation. SST changes are also different, with increases over the Arabian Sea and BoB in CFSv2 (and decreases further south and along the eastern coast of India) and decreases everywhere in GloSea.

210   Days 31 to 50 show very little change in GloSea, whereas there is much more change in CFSv2, which has an increase in westerly flow over India and an increase in cyclonic flow over eastern India and the northern BoB. This is similar to what is seen in GloSea over the previous two periods, and is accompanied by an even stronger increase in precipitation. The precipitation decreases to the south of India so that overall the change is in the opposite direction (and stronger) to that in the previous period in CFSv2. The SST and precipitation changes match very closely in CFSv2, except over the very north of the

215   BoB and Bangladesh and eastern India, and along the western coast of India.

Days 50 to 101 also show little change in GloSea, with small decreases in precipitation in northern India and small increases in southern India. The flow into the southern part of the western side of the box changes direction somewhat so that more is coming into the western part of the southern side of the box. There is much more change in CFSv2, with a substantial reduction

in precipitation; the pattern looks similar to that in GloSea during days 3 to 8, but with the anticyclonic flow difference and the strongest precipitation reduction centred further west, over the Arabian Sea. The SST and precipitation differences again look remarkably similar in CFSv2.

From day 101 onwards, both systems have roughly constant precipitation within the analysis region used in Fig. 1 but, whereas in GloSea there is very little change in the wind or precipitation fields, in CFSv2 there are changes in both wind and precipitation fields, with the precipitation changes cancelling each other when averaged over the region as a whole. In CFSv2 there is a reduction in westerly flow over India, which seems to cause a reduction in precipitation over the western coast, but an increase over the peninsula, so it could be that less moist air is advected out to the east. Both systems show widespread decreases in SST.

3.3 Behaviour during different parts of the monsoon season

The development with lead time for different parts of the monsoon season is shown in Fig. 8. Because the CFSv2 hindcasts are only available initialised from February, the longest lead times are not available in June and July. All three months show sharp initial decreases. In June this is followed by a consistent but decelerating decrease throughout the length of the hindcast. The recovery followed by a further decrease seen for CFSv2 is present in all months, but is much stronger in July and August. The less substantial recovery behaviour seen for GloSea also occurs in all months, but in August on somewhat longer time scales: the worst low-precipitation biases are seen for lead times of 8-50 days, with the bias reducing to a smaller value from 50 to 100 days. It is also notable that the differences between the three model setups are much larger in July and August than in June.
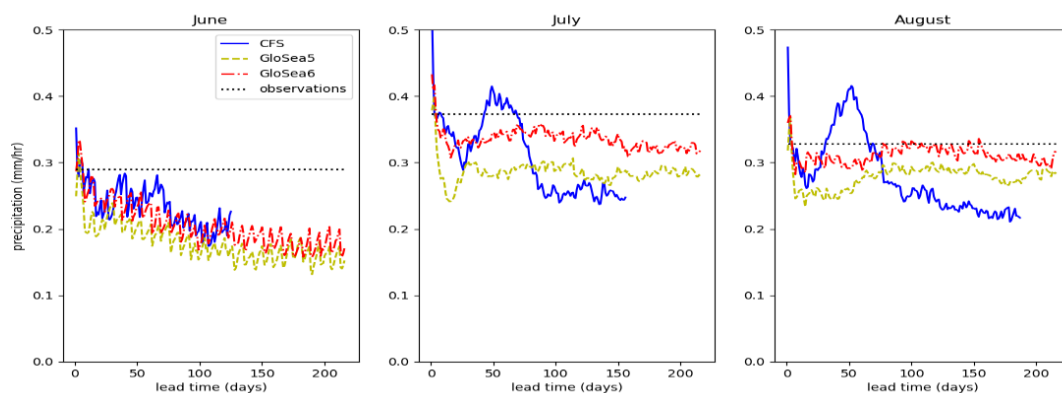
Figure 8: Variation of precipitation with hindcast lead time (averaged over 8N–29N and 69E–89E and 2012–2015) for hindcasts valid in each of June, July and August. The dotted lines show observed values averaged over all dates in the month (i.e., not just dates on which hindcasts are available).

The behaviour in different parts of the season in GloSea is consistent with the findings of Martin & Levine (2012), who evaluated the seasonal cycle of precipitation over a similar region to that used in this study for climate simulations using an earlier version of the GC model. Looking at the recent past climate, they found both atmosphere-only (forced by observed

SSTs) and coupled-model simulations to produce too little precipitation over the region throughout June–August, but with the
245   bias being worse in the coupled simulation earlier in the period, and worse in the atmosphere-only simulation later in the
period. The early poorer performance of the coupled simulation was attributed to a delayed monsoon onset caused by cold
SST biases over the Arabian Sea, as described by Levine & Turner (2012). Meanwhile, the later better performance of the
coupled simulation was attributed to a cold SST bias over EIO associated with reduced precipitation there, leading to increased
precipitation over the Indian Peninsula.

250   Figure 9 shows that there is a cold SST bias in GloSea5 over the Arabian Sea in June, which becomes larger as the lead time
increases. In other words, the earlier in the year that the seasonal hindcast is initialised, the longer the SST bias has to develop
over the course of the simulation, which, based on Levine & Turner (2012), leads to a more delayed onset and therefore a
larger low-precipitation bias.
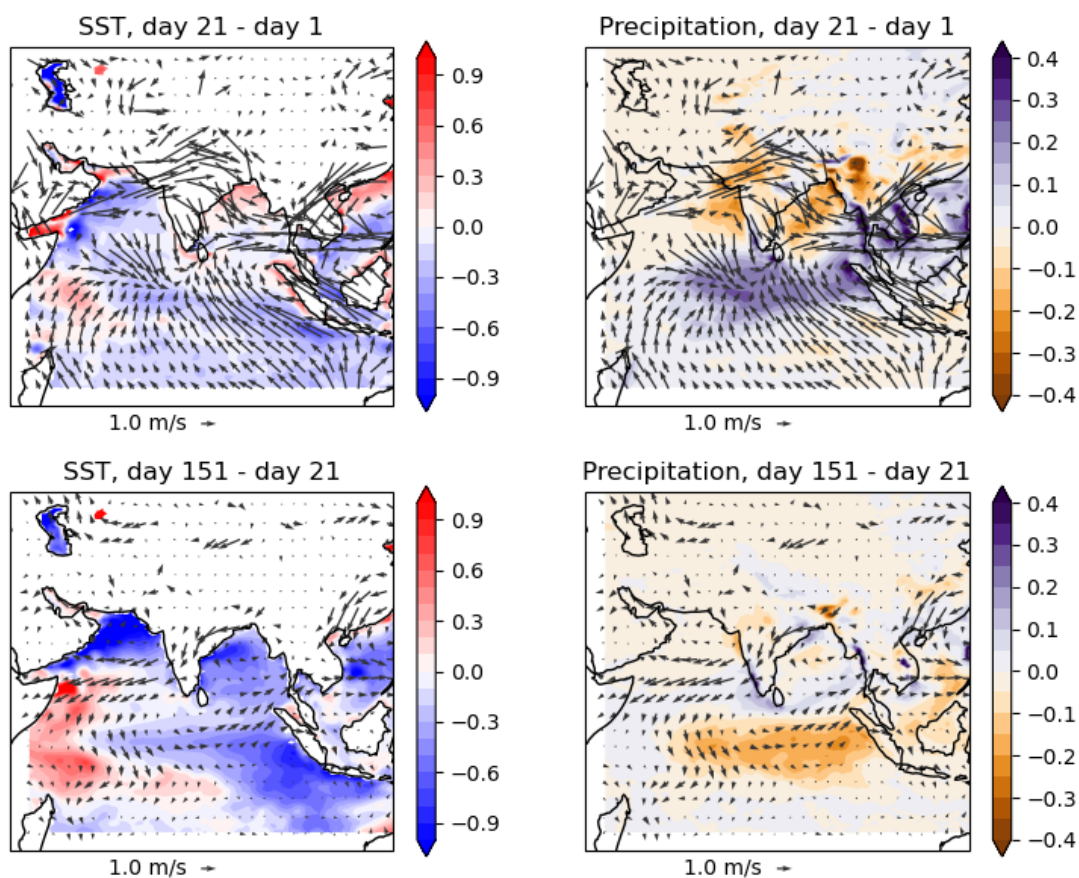
255   **Figure 9: Changes in SST (K), precipitation (mm/hr) and wind in GloSea5 for valid times in June, between the lead times shown.**

Meanwhile, for August valid times the situation is slightly more complex. At short lead times biases in the atmospheric component of the model mean that the low-precipitation bias is larger if the hindcast has been started earlier for a given valid time. At longer lead times, however, initialising the hindcast earlier in the season means that the cold SST bias over EIO has had longer to develop, counteracting the early high-precipitation bias there (indeed, the excess precipitation may itself

260   contribute to the cold SST bias via excess wind stresses, as discussed by Levine & Turner, 2012), and mitigating the low-precipitation bias over India. This is illustrated in Fig. 10: at 20 days' lead time, there has been a small decrease in EIO SSTs, but much increased convergence into the EIO and increased precipitation there. From 20-150 days, however, the cold EIO SST bias is much more fully developed and the previous south-eastward change in the flow during the first 20 days has now been reversed. There is decreased precipitation over EIO and increased flow from EIO into southern India leading to increased

265   precipitation over the western coast of India.

Figure 10: Changes in SST (K), precipitation (mm/hr) and wind in GloSea5 for valid times in August, between the lead times shown.

3.4 Variation with BSISO phase at hindcast valid time

The hindcasts are categorised according to the observed BSISO phase at the valid time, following Keane et al. (2021), taking

270   precipitation averaged over latitudes 8N–29N and 69E–89E. For each lead time, all hindcasts where the observed BSISO amplitude at valid time is greater than 1 are assigned a phase equal to the observed phase on the date at that lead time (those with amplitude less than or equal to 1 are discarded for this method). For each phase, an average is taken of all the area-averaged precipitation values to produce a quantity that varies as a function of BSISO phase and lead time. This quantity is plotted as a function of phase in Fig. 11, for selected lead times, with a further 8-day average over lead time to reduce noise.

275   Also plotted is the quantity for observations, which applies the same method (including the restriction to BSISO amplitudes greater than 1) to observed precipitation over all days during June–August 2002–2015. Versions of Fig. 11 using fewer GloSea

members and using a longer range of GloSea years are shown in Appendix A (Figs. A9 and A10, respectively), and are very similar.

Looking at GloSea5 during the first 8 days, the bias is worse for phases where the large-scale dynamics implies increasing precipitation and less bad when the large scale dynamics implies decreasing precipitation, in agreement with the findings of Keane et al. (2021) for 7-day forecasts. The situation is slightly different for GloSea6 and CFSv2, with the precipitation generally still too high when averaged over the first 8 days of the hindcast, but there is the same shift in the peak precipitation from phase 4 in the observations to phase 5 in all the models.
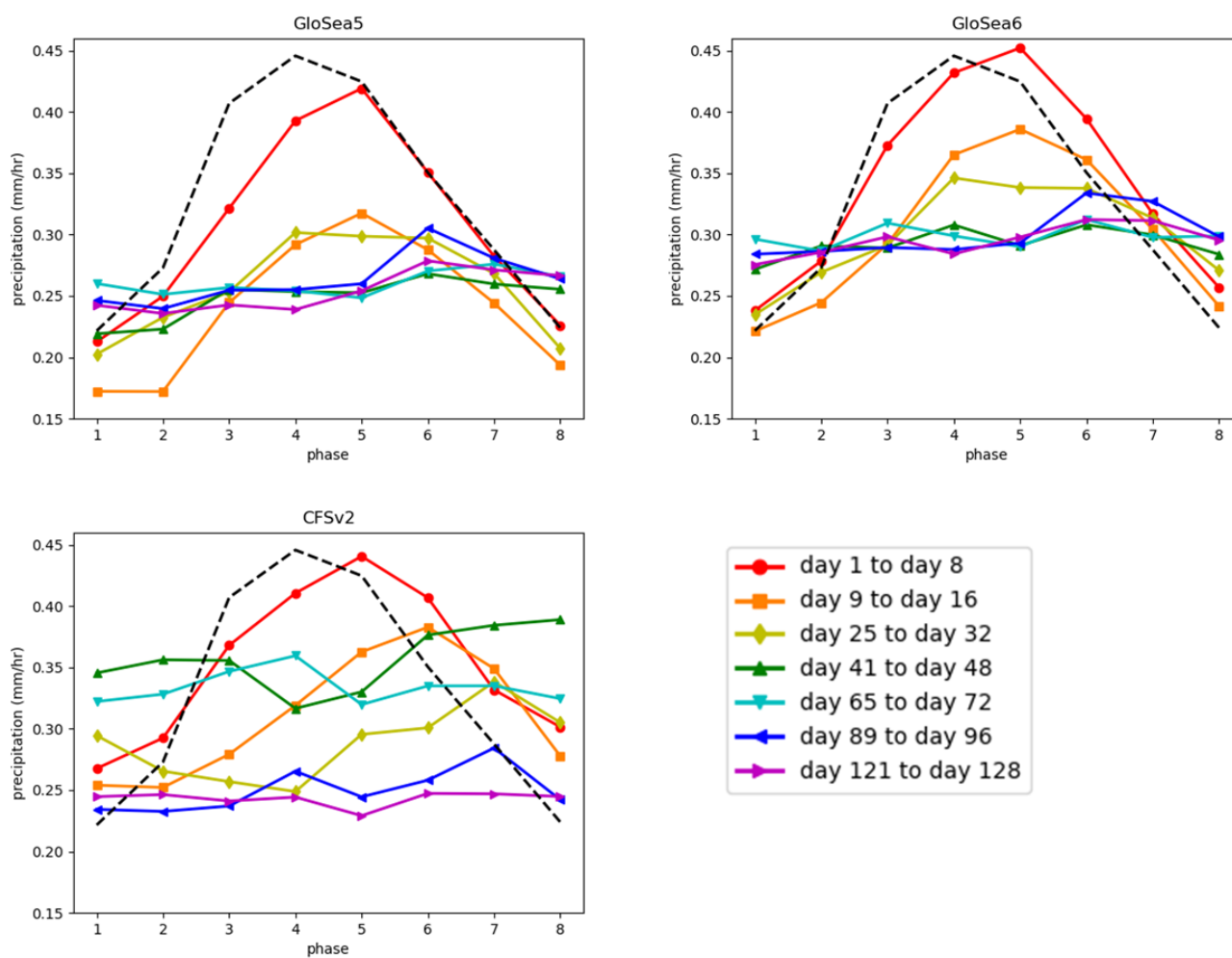
Figure 11: Variation in precipitation (averaged over 8N–29N and 69E–89E and June–August 2012–2015) with lead time as a function of observed BSISO phase at valid time, averaged over 8-day lead time blocks (coloured lines). Each panel corresponds to a model denoted by its title. Observed precipitation corresponding to each BSISO phase is denoted by the black dashed line in all three panels.

Comparing the second 8 days with the first 8 days for all models, it is clear that the behaviour continues, with generally a
285 reduction for all phases, but a stronger reduction when the large-scale dynamics implies increasing precipitation and vice-
versa. From day 16 this continues but becomes weaker as the hindcasts lose their phase dependence until at day 40 the errors
are essentially independent of phase. This suggests that the models lose their capability to forecast the BSISO phase by 40
days into the hindcast, as the model precipitation (and, therefore, any BSISO phase that it is simulating) has no significant
relationship with the observed BSISO phase. This is consistent with previous work that has shown that seasonal forecast
290 models can effectively simulate the BSISO on time scales of tens of days (e.g., Lee et al., 2015; Fang et al., 2019).

3.5 Variation with BSISO phase at initial time

In order to establish the role of initial conditions on the development of the rainfall biases over India in the two seasonal
forecast systems, hindcasts initialised from 1st June to 1st August (inclusive), for each year, are next categorised according to
the observed BSISO phase at the start of the hindcast. The precipitation is again averaged over latitudes 8N–29N and 69E–
295 89E, and over all hindcasts corresponding to each phase, and values for the first 60 hindcast days in each system are plotted in
Fig. 12. For this method there is no temporal coarse-graining into 8-day blocks; therefore, no minimum restriction on the
BSISO amplitude is applied, so that a larger data sample can be taken to reduce random temporal fluctuations that would
otherwise be reduced by the 8-day coarse-graining. The dotted lines show observed values averaged over the same dates on
which each length of hindcast is available; as for Fig. 1, this is different between the two systems as the hindcasts are initialised
300 on different dates. Figure A11 shows a similar set of plots, but also including hindcasts initialised in the rest of August, and

extending only to 30 days: these plots from a somewhat larger sample size are in broad agreement with the first 30 days of those in Fig. 12.
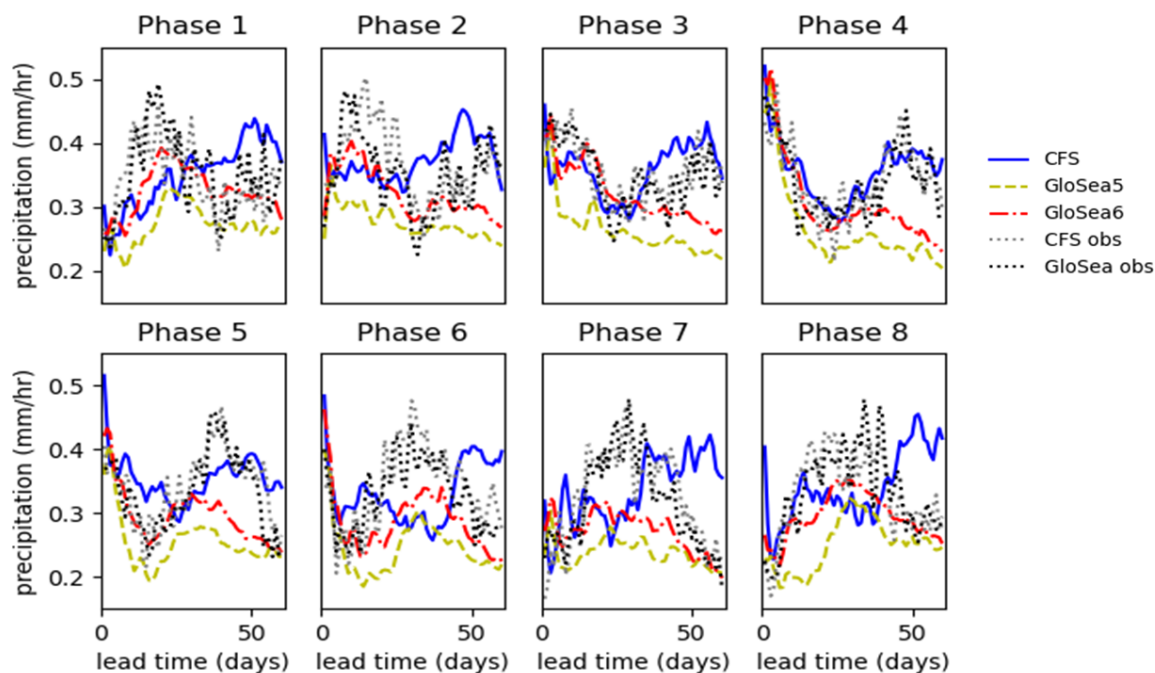
Figure 12: Variation in precipitation with hindcast time, for hindcasts initialised during each of 8 BSISO phases. Values are averaged over 8N–29N and 69E–89E and over hindcasts initialised during the period 1st June to 1st August 2012–2015 on dates where the observed BSISO was in the given phase. The black dotted lines show observed values averaged over the same dates as the hindcasts at the relevant lead time.

We use the observed curves to define how the large-scale drivers affect the precipitation through the course of each hindcast, and they are similar to what is expected from the standard dynamical analysis that is used to define the phases. For example, hindcasts starting in phase 4 have high initial precipitation on average, and this decreases early in the hindcast, while those starting in phase 8 have low initial precipitation on average, and this increases early in the hindcast. Moreover, the curves follow an oscillation in precipitation with a period of about 40 days, corresponding to the period of the BSISO cycle.

A general conclusion from Fig. 12 is that both models perform better when the large-scale dynamics is driving decreases in precipitation than when it is driving increases in precipitation. For example, the first 30 days are well simulated when the hindcast starts in phases 4 or 5, whereas the precipitation is far too low over the first 30 days when the hindcast starts in phases 8, 1 or 2, particularly for GloSea5 (CFSv2 sometimes even simulates too much precipitation, although this is usually associated with an initial high-precipitation bias). This continues further into the hindcast in GloSea: for phases 4 and 5, although the first 30 days are well simulated, the subsequent observed increasing precipitation is not well captured, and the improvement in GloSea6 compared to GloSea5 in capturing increasing precipitation is less than that during the first 30 days of the hindcast (e.g., phases 8, 1, 2). CFSv2 does simulate the later increase for phases 4 and 5, although this could be because it produces increasing precipitation more generally during days 30 to 50 of the hindcast.

4 Conclusions

This study investigates Indian summer monsoon biases in two seasonal forecasting systems, CFSv2 and versions 5 and 6 of GloSea. Both systems initially have a reduction in precipitation with increasing lead time, accompanied by increasingly anti-
320 cyclonic flow, and in GloSea the precipitation reduction is shown to fully occur within the first 8 days of the hindcast. This this corroborates previous work (e.g., Rodwell and Palmer, 2007; Martin et al., 2010; Rodriguez and Milton, 2019; Martin et al., 2021) showing that future work studying biases in weather forecasts (and, more generally, short-time-integration simulations) will provide substantial insight into biases across timescales, without the requirement to conduct lengthy climate simulations, particularly for the GC system. Both systems show a substantial decrease within a lead time of 25 days, and the
325 results for GloSea are in broad agreement with previous work on atmosphere-only weather forecasts. This suggests that issues in the atmospheric model component of the system are sufficiently important that atmospheric-only simulations can continue to play a role in investigating these biases.

It is notable that GloSea6 has improved (i.e., smaller) biases compared to GloSea5. Although the Indian summer monsoon low-precipitation bias is an important factor in evaluating the performance of GC3 compared with GC2, improvements in GC
330 versions are aimed at Global model performance as a whole and on the full range of time scales, from weather forecasting to climate simulation. It is therefore encouraging that the combined effect of these improvements on the simulation of the Indian summer monsoon on seasonal time scales has been so substantially positive. The upgrade from GC2 to GC3 (Williams et al., 2017) includes a wide range of improvements to the atmosphere and land components (Walters et al. 2017), the ocean component (Storkey et al., 2017) and the sea ice component (Ridley et al., 2017). In particular, the previous upgrade in the
335 atmospheric component (GA6) had focused on the dynamical core, with changes to the physics parameterisations relatively restricted, so that the upgrade from GA6 (used in GC2) to GA7 (used in GC3) included a relatively large number of substantial longer-term changes to the atmospheric parameterisation schemes.

After its initial reduction, the precipitation recovers in CFSv2, so that it is in agreement with observations over lead times of 30–70 days. It could therefore be interesting to study this recovery period further: although it is based on errors in the model
340 (as quantities should not vary with forecast/hindcast lead time as plotted in Fig. 1), this could provide insight into conditions under which the model is capable of simulating break-to-active transitions. A similar, albeit much smaller and more short-lived, recovery is also identified in GloSea, suggesting that such insight could apply to different modelling systems.

Although the biases seem to initially develop from issues in the atmospheric model components, the interaction with SSTs in the ocean component is also important. In CFSv2 this interaction seems to be quite direct (with decreasing SSTs corresponding
345 closely with decreasing precipitation), and perhaps more important than in GloSea, where it seems to depend more strongly on the part of the season that is evaluated. This could be due to differences in the two ocean model components or in the coupling between the atmosphere and the ocean; Bollasina and Nigam (2009) showed that different coupled models exhibit varyingly deficient representation of local and non-local air–sea interactions in the Indian Ocean during boreal summer and, in particular, that they tend to overestimate the correlation between SST and precipitation, suggesting that local air–sea

350 interactions are overemphasised. Meanwhile, when focussing on June, the behaviour of the two systems (and the two versions of GloSea) is much more similar, and suggests that both systems suffer from a delayed monsoon onset, so this could be a common issue affecting both systems in the same way.

An analysis of how the seasonal forecast total precipitation amount depends on observed BSISO state has been carried out in this study, in terms of both the phase at the beginning of the forecast and the phase at the end of the forecast. Both evaluation

355 methods show that the two systems are best at simulating situations where the large-scale dynamics favours decreasing precipitation over India, and are worst at simulating situations where the large-scale dynamics favours increasing precipitation over India, and that this continues beyond the first 8 days of the forecast and even into a second BSISO cycle. This suggests an opportunity to focus future work on cases corresponding to such increasing precipitation conditions, and it will be interesting to investigate how widespread the behaviour is amongst other models. It also provides useful information to users on the

360 relative reliability of forecasts of each of these transitions.

One explanation for the dependence on BSISO phase could be that, based on their systematic biases, the two systems have a tendency to move towards monsoon break conditions and so are better at capturing situations where this is occurring in reality. Further analysis of such transitions in the models may provide insight into the reasons for this preference and its contribution to the overall systematic biases in Indian summer monsoon rainfall in climate models. Gera et al. (2021) evaluated seasonal

365 forecasts of the Indian summer monsoon using the NCMRWF-ERP system based on GC2 and found that, while break-to-active and active-to-break transitions were both predicted well up to 4 weeks, there was some evidence of a weakening and a delay in the break-to-active transitions with increased forecast lead time.

The BSISO analysis also shows that the precipitation in both systems is largely independent of observed BSISO state by about 40 days into the forecast. It will therefore be interesting in future work to carry out a similar analysis of how the biases vary

370 with the models' own BSISO state and, indeed, to what extent the models are able to simulate the BSISO, and determine whether similar variation of bias with BSISO phase extends further into the forecast. It may also be useful to use the longer-range predictability of the BSISO phase to add information about likely biases in weather and seasonal forecasts, particularly if the BSISO is not well simulated by the models, in which case this information would not already be included in the forecasts themselves.

375 As already mentioned, the purpose of seasonal forecasts is largely to produce a statistical idea of the state of the weather a few weeks to months ahead, and the hindcasts evaluated in this study are in practice used to calibrate the actual forecast models, so that systematic biases should not directly affect the quality of the forecast. However, it may be of interest in future work to investigate whether there is any relationship between model bias and forecast skill in the seasonal forecasts.

Appendix A: Additional figures and table

Initialization month	Dates
February	05, 10, 15, 20, 25 (00 &12 UTC)
March	02, 07, 12, 17, 22, 27 (00 & 12 UTC)
April	01, 06, 11, 16, 21, 26 (00 & 12 UTC)
May	06, 11, 16, 21, 26 (00 & 12 UTC)
June	05, 10, 15, 20, 25 (00 &12 UTC)
July	05, 10, 15, 20, 25 (00 &12 UTC)
August	05, 10, 15, 20, 25 (00 &12 UTC)

380

Table A1: Start dates of CFSv2 hindcasts evaluated in this study.
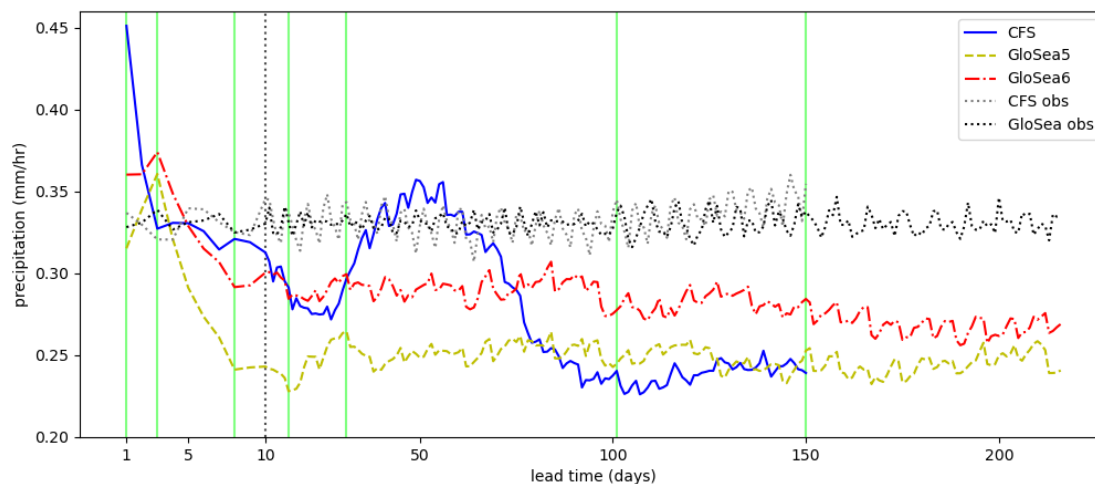
Figure A1: As Fig. 1 but with only 3 of the 7 ensemble members in GloSea.
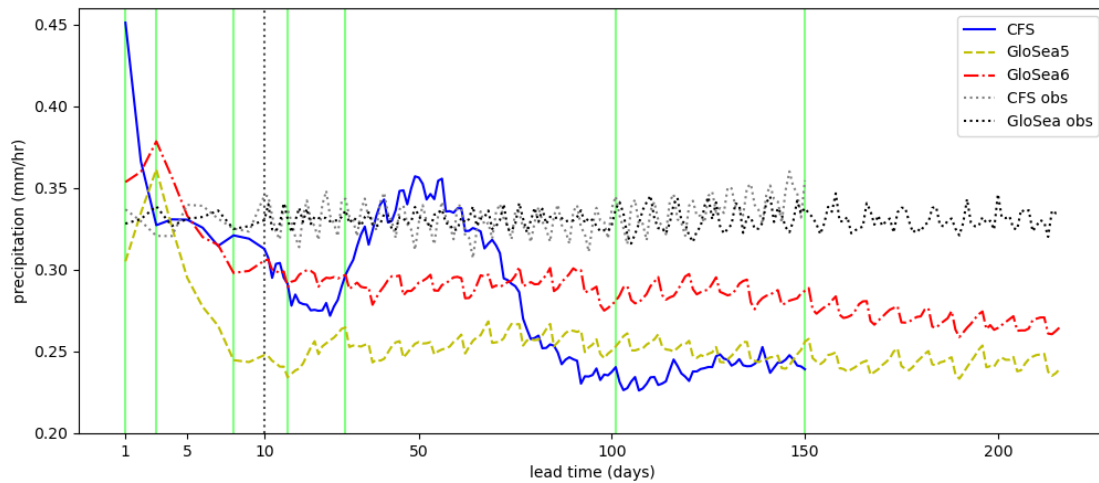
Figure A2: As Fig. 1 but with GloSea5 hindcasts valid during 1994–2015 and GloSea6 hindcasts valid during 1994–2016 (all other data unchanged, i.e., "GloSea obs" still refers to the period 2002–2015).
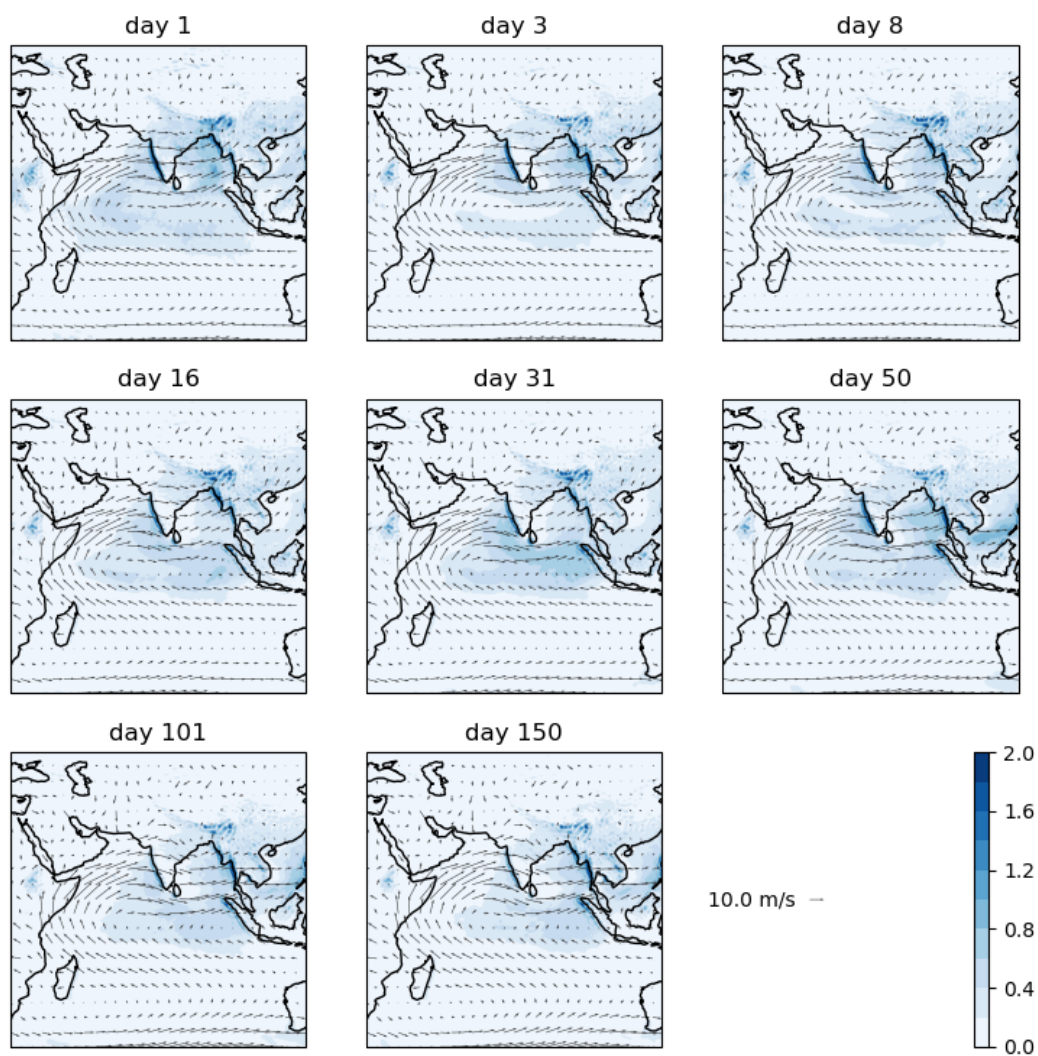
Figure A3: Precipitation (colours, in mm/hr) and 850-hPa wind (vectors) in CFSv2, at the hindcast lead time shown, averaged over June–August 2012–2015.
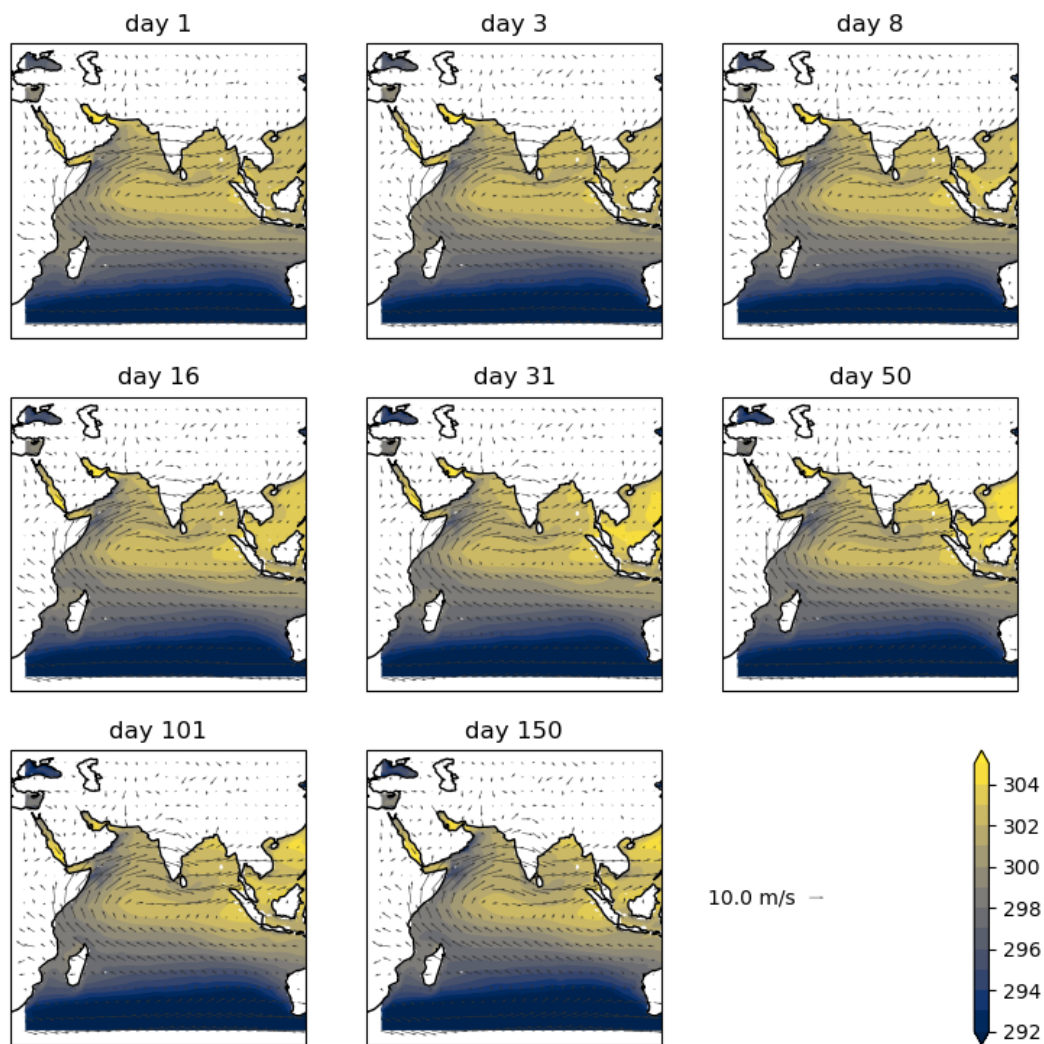
Figure A4: SST (colours, in K) and 850-hPa wind (vectors) in CFSv2, at the hindcast lead time shown, averaged over June–August 2012–2015.
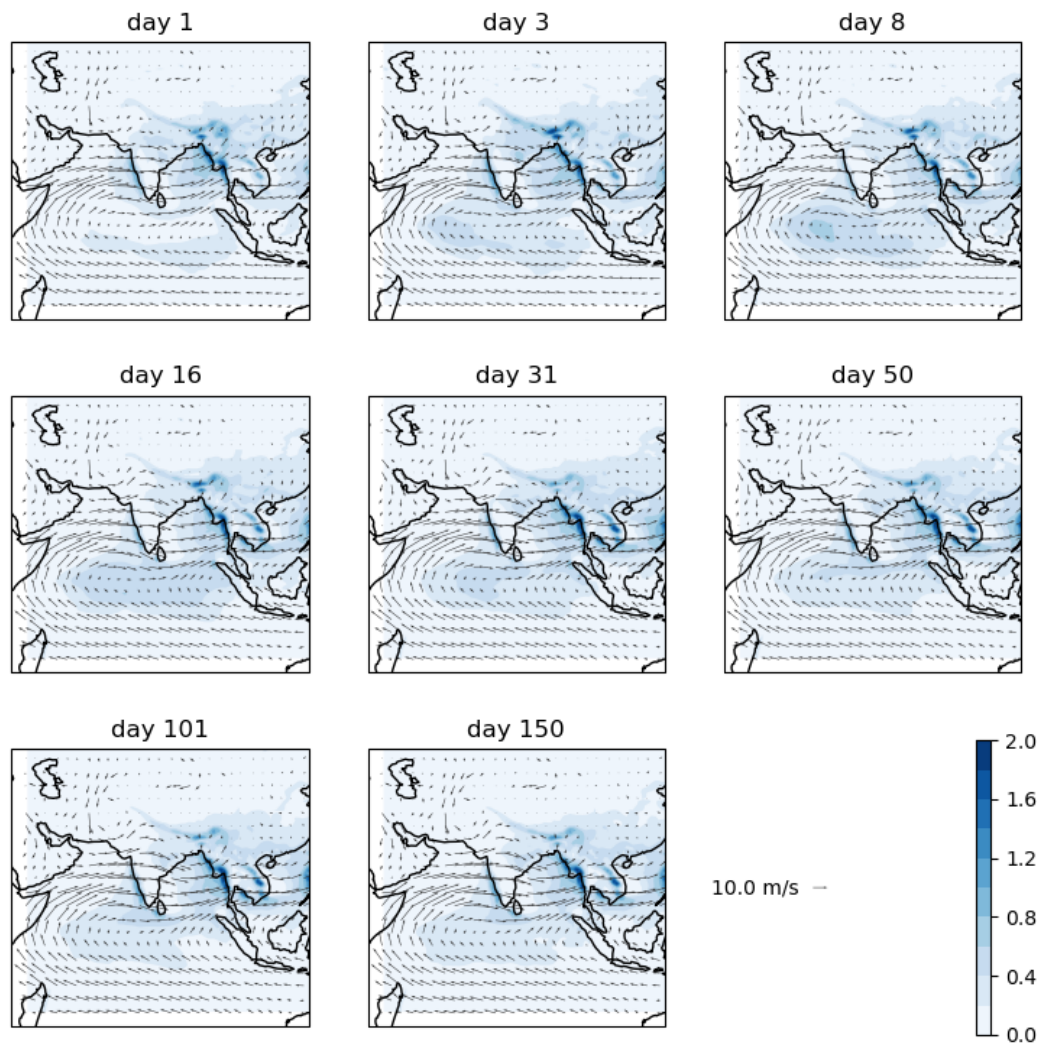
Figure A5: Precipitation (colours, in mm/hr) and 850-hPa wind (vectors) in GloSea5, at the hindcast lead time shown, averaged over June–August 2012–2015.
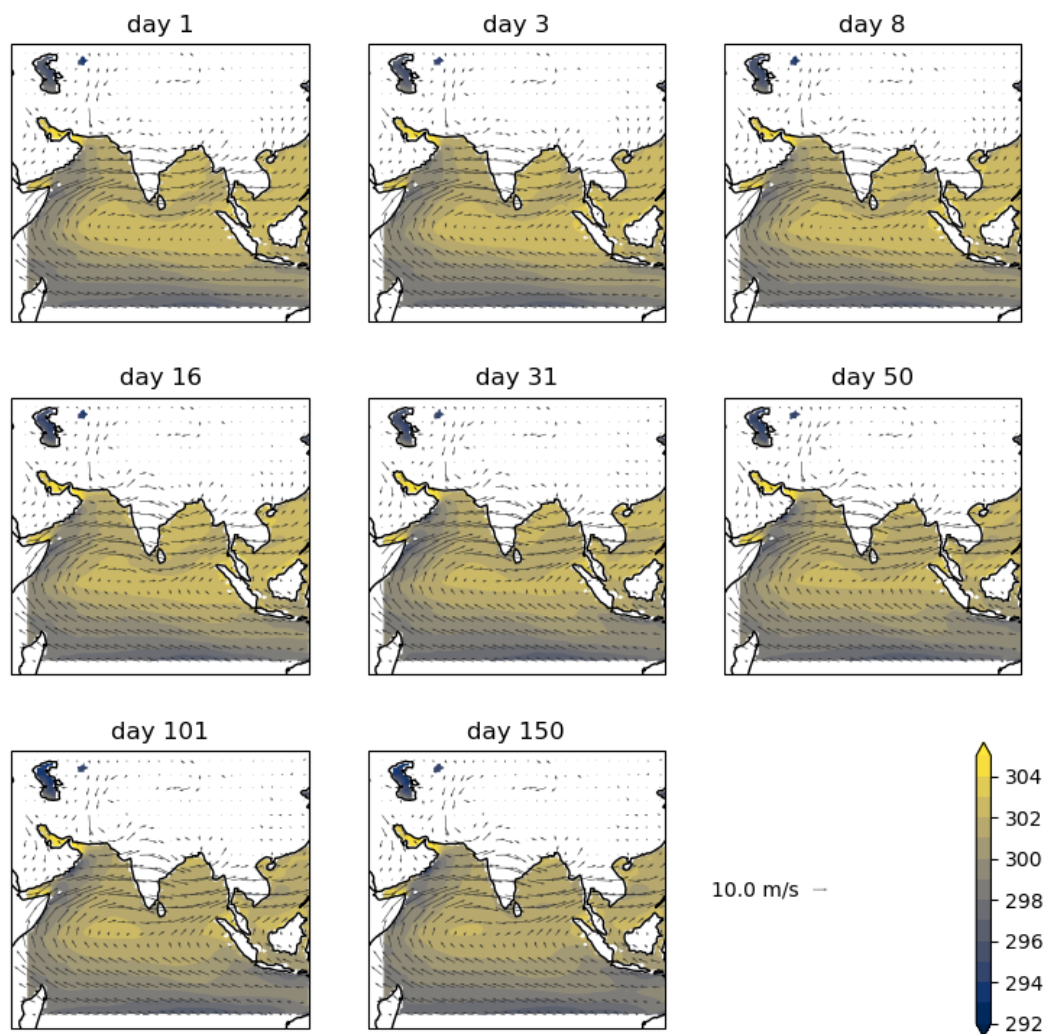
Figure A6: SST (colours, in K) and 850-hPa wind (vectors) in GloSea5, at the hindcast lead time shown, averaged over June–August 2012–2015.
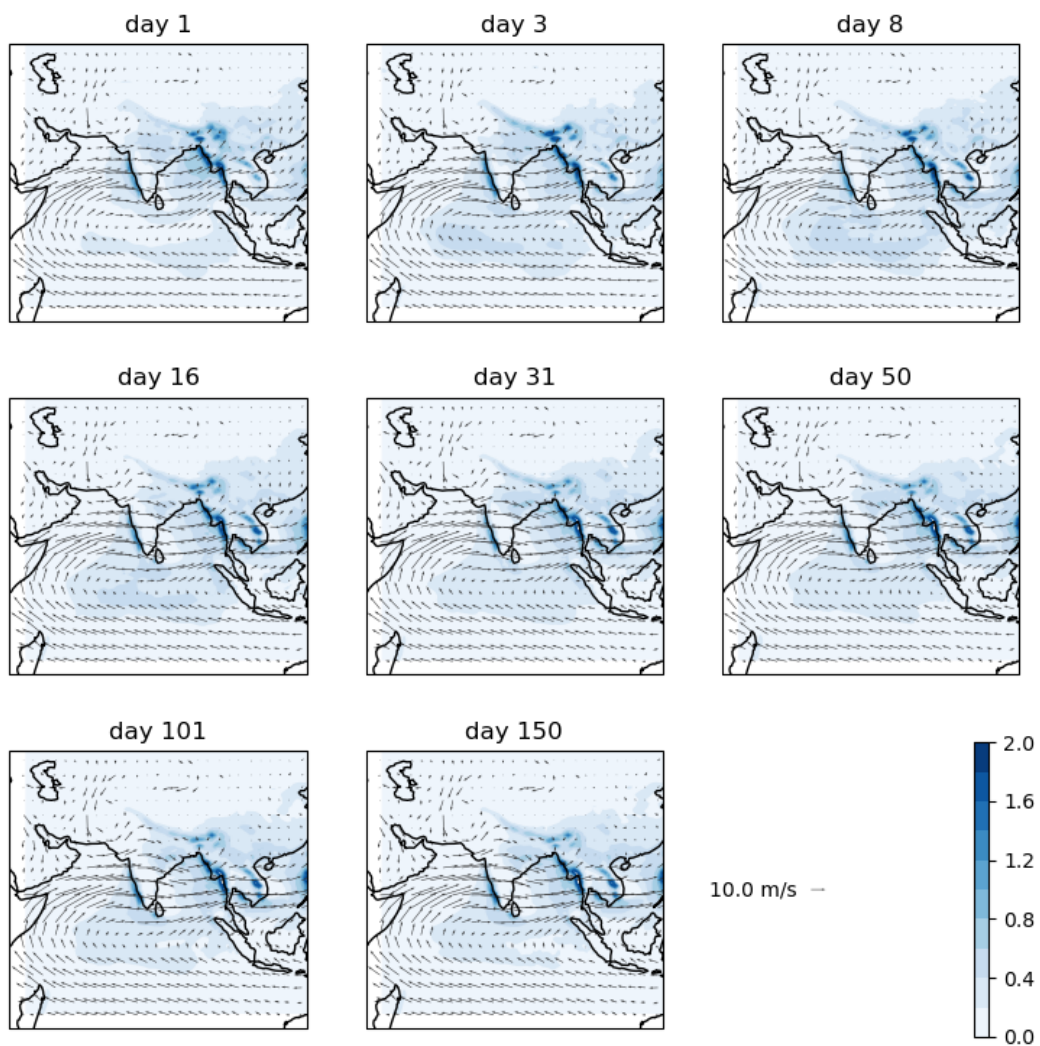
400

Figure A7: Precipitation (colours, in mm/hr) and 850-hPa wind (vectors) in GloSea6, at the hindcast lead time shown, averaged over June–August 2012–2015.
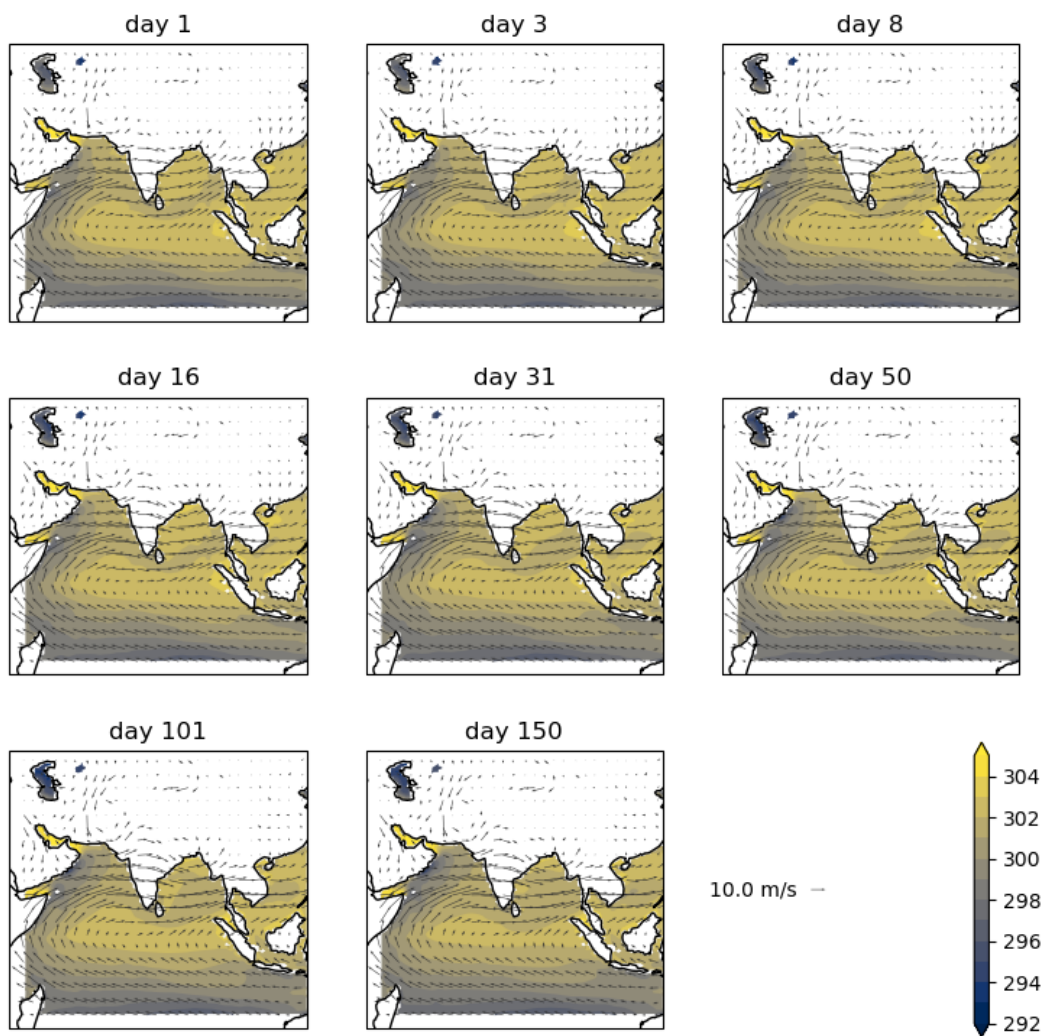
Figure A8: SST (colours, in K) and 850-hPa wind (vectors) in GloSea6, at the hindcast lead time shown, averaged over June–August 2012–2015.

405
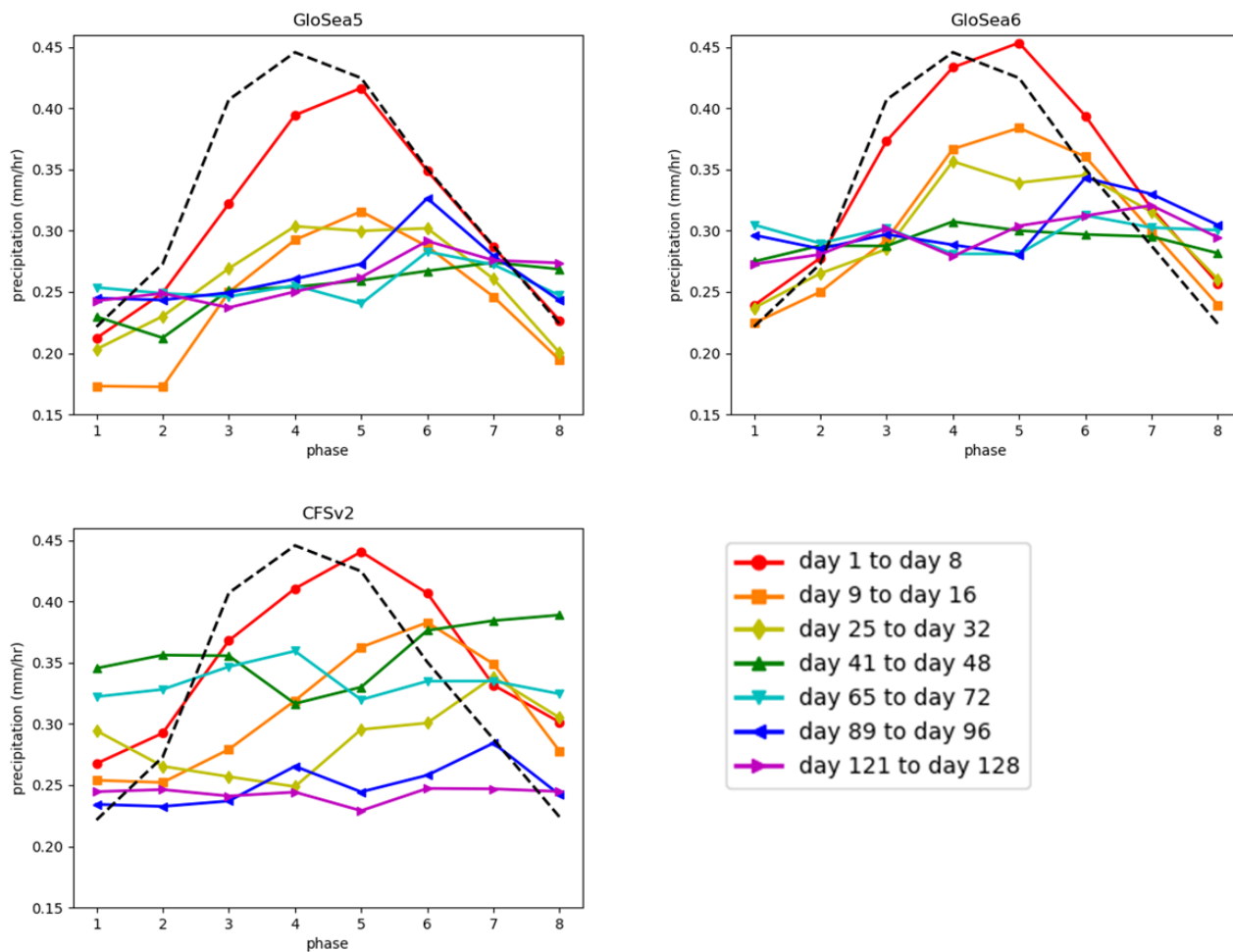
Figure A9: As Fig. 11 but with only 3 of the 7 ensemble members in GloSea.
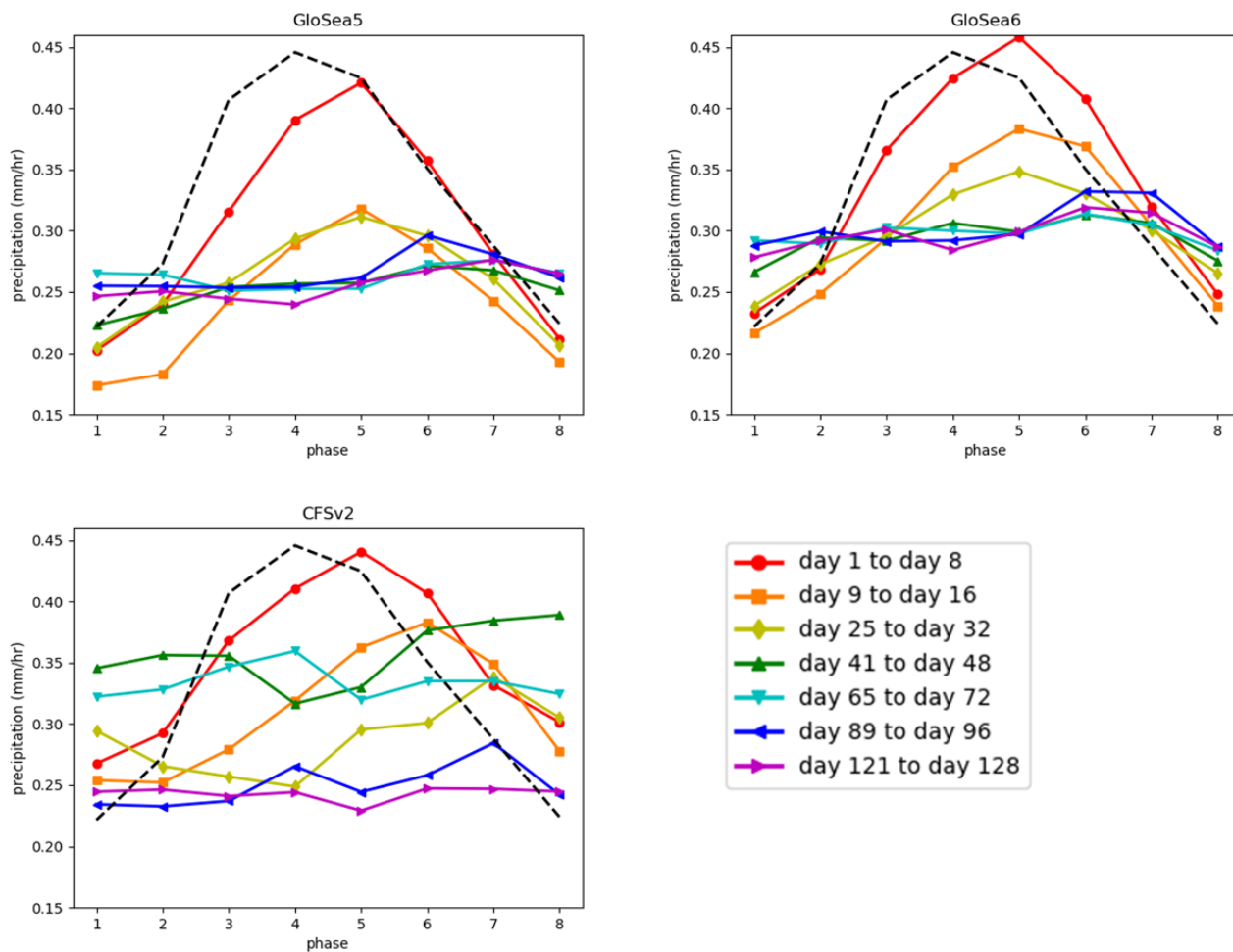
Figure A10: As Fig. 11 but with GloSea5 hindcasts valid during 1994–2015 and GloSea6 hindcasts valid during 1994–2016 (all other data unchanged, i.e., the black dashed lines refer to observations during 2002–2015 in all three panels).
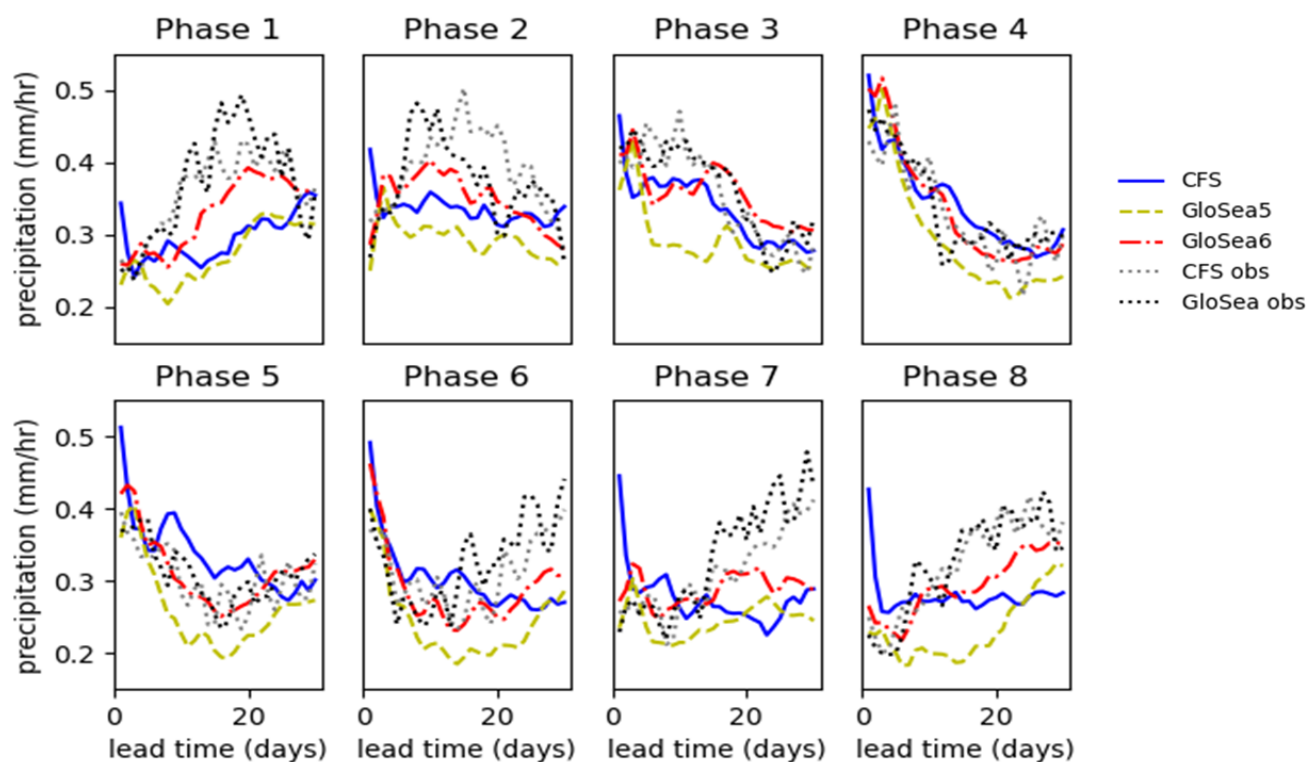
Figure A11: As Fig. 12 but including start dates up to 31st August and only to 30 days' hindcast time.

Code availability

Due to intellectual property right restrictions, we cannot provide either the source code or documentation papers for the Met Office Unified Model (MetUM). The MetUM is available for use under licence. For further information on how to apply for a licence, see https://www.metoffice.gov.uk/research/approach/collaboration/unified-model/partnership. JULES is available under licence free of charge. For further information on how to gain permission to use JULES for research purposes, see https://jules.jchmr.org/. The model code for NEMO v3.4 is available from the NEMO Consortium and can be downloaded from their repository (https://forge.ipsl.jussieu.fr/nemo/chrome/site/doc/NEMO/guide/html/install.html; https://doi.org/10.5281/zenodo.1464816; NEMO System Team, 2020). The model code for CICE is freely available from the CICE Consortium, a group of stakeholders and primary developers of the Los Alamos sea ice model, and can be downloaded from the CICE repository (https://github.com/CICE-Consortium/CICE/wiki). To obtain source code and documentation for CFSv2, see https://www.tropmet.res.in/monsoon/monsoon2/MM_Model_CFS_Output.php. Model data used in this study are available to research collaborators upon request. Observed precipitation data were obtained from

ftp://arthurhou.pps.eosdis.nasa.gov/pub/gpmdata/YYYY/MM/DD/imerg/ and observed BSISO data were taken from https://iprc.soest.hawaii.edu/users/kazuyosh/ISO_index/data/BSISO_25-90bpfil_pc.extension.txt.

Author contribution

430 RJK designed the evaluation, with contributions from all authors. AS generated and evaluated the CFSv2 hindcasts and RJK evaluated the GloSea hindcasts. RJK prepared the manuscript, with contributions from all authors.

Competing interests

The authors declare that they have no conflict of interest.

Acknowledgements

435 R.J. Keane and G.M Martin were funded by the Met Office Weather and Climate Science for Service Partnership (WCSSP) India project which is supported by the UK Department for Science, Innovation & Technology (DSIT). WCSSP India is a collaborative initiative between the Met Office and the Indian Ministry of Earth Sciences (MoES). A. Srivastava is supported by the Indian Institute of Tropical Meteorology, Ministry of Earth Sciences, Pune, India. The IMERG data were provided by the NASA/Goddard Space Flight Center and PPS, which develop and compute IMERG as a contribution to GPM, and archived
440 at the NASA GES DISC.

References

Abhilash, S., Sahai, A. K., Borah, N., Chattopadhyay, R., Joseph, S., Sharmila, S., De, S., Goswami, B. N., and Kumar, A.: Prediction and monitoring of monsoon intraseasonal oscillations over Indian monsoon region in an ensemble prediction system using CFSv2, Clim. Dyn., 42, 2801–2815, https://doi.org/10.1007/s00382-013-2045-9, 2014.

445 Bollasina, M. and Nigam, S.: Indian Ocean SST, evaporation, and precipitation during the South Asian summer monsoon in IPCC-AR4 coupled simulations, Clim. Dyn., 33, 1017–1032, https://doi.org/10.1007/s00382-008-0477-4, 2009.

Bowler, N. E., Arribas, A., Beare, S. E., Mylne, K. R. and Shutts, G. J.: The local ETKF and SKEB: Upgrades to the MOGREPS short-range ensemble prediction system, Q. J. R. Meteorol. Soc., 135, 767-776, https://doi.org/10.1002/qj.394, 2009.

450 Chattopadhyay, R., Rao, S. A., Sabeerali, C. T., George, G., Rao, D. N., Dhakate, A. and Salunke, K.: Large-scale teleconnection patterns of Indian summer monsoon as revealed by CFSv2 retrospective seasonal forecast runs, Int. J. Climatol., 36, 3297-3313, https://doi.org/10.1002/joc.4556, 2016.

Chevuturi, A., Turner, A. G., Woolnough, S. J., Martin, G. M., and MacLachlan, C.: Indian summer monsoon onset forecast skill in the UK Met Office initialized coupled seasonal forecasting system (GloSea5-GC2), Clim. Dyn., 52, 6599–6617,
455   https://doi.org/10.1007/s00382-018-4536-1, 2019.

Choudhury, B. A., Rajesh, P. V., Zahan, Y., and Goswami, B. N.: Evolution of the Indian summer monsoon rainfall simulations from CMIP3 to CMIP6 models, Clim. Dyn., 58, 2637–2662, https://doi.org/10.1007/s00382-021-06023-0, 2022.

Fang, Y., Li, B., and Liu, X.: Predictability and Prediction Skill of the Boreal Summer Intra-Seasonal Oscillation in BCC_CSM Model, Journal of the Meteorological Society of Japan. Ser. II, 97, 295-311, https://doi.org/10.2151/jmsj.2019-019, 2019.

460   Gautam, P., Chattopadhyay, R., Joseph, S., Martin, G. M., and Sahai, A. K.: Coupled model biases and extended-range prediction skill during the onset phase of the Indian summer monsoon with different initializations related to land surface and number of observations, Quarterly Journal of the Royal Meteorological Society, 149(754), 1650–1673, https://doi.org/10.1002/qj.4475, 2023.

George, G., Rao, D. N., Sabeerali, C. T., Srivastava, A., and Rao, S. A.: Indian summer monsoon prediction and simulation in
465   CFSv2 coupled model, Atmos. Sci. Lett., 17, 57-64, https://doi.org/10.1002/asl.599, 2016.

Gera, A., Gupta, A., Mitra, A. K., Rao D., N., Momin, I. M., Rajeeavan, M.N., Milton, S. F., Martin, G. M., Martin, M. J., Waters, J., and Lea, D.: Skill of the extended range prediction (NERP) for Indian summer monsoon rainfall with NCMRWF global coupled modelling system, Q. J. R. Meteorol. Soc., 148(742), 480–498, https://doi.org/10.1002/qj.4216, 2021.

Huffman, G. J., E. F. Stocker, D. T. Bolvin, E. J. Nelkin, and Tan, J.: GPM IMERG Final Precipitation L3 Half Hourly 0.1
470   degree x 0.1 degree V06, Greenbelt, MD, Goddard Earth Sciences Data and Information Services Center (GES DISC), 10.5067/GPM/IMERG/3B-HH/06, 2019.

Jain, S., Scaife, A. A., and Mitra, A. K. Skill of Indian summer monsoon rainfall prediction in multiple seasonal prediction systems, Clim. Dyn., 52, 5291–5301, https://doi.org/10.1007/s00382-018-4449-z, 2019.

Johnson, S. J., Turner, A., Woolnough, S., Martin, G., and MacLachlan, C.: An assessment of Indian monsoon seasonal
475   forecasts and mechanisms underlying monsoon interannual variability in the Met Office GloSea5-GC2 system, Clim. Dyn., 48, 1447–1465, https://doi.org/10.1007/s00382-016-3151-2, 2017.

Joseph, S., Chattopadhyay, R., Sahai, A. K., Martin, G. M., Dey, A., Mandal, R., and Phani, R.: Evaluation and comparison of the subseasonal prediction skill of Indian summer monsoon in IITM CFSv2 and UKMO GloSea5, Clim. Dyn., 61, 1683–1696, https://doi.org/10.1007/s00382-022-06650-1, 2023.

480   Kar, S.C., Joshi, S., Shrivastava, S., and Tiwari, S.: Dynamical characteristics of forecast errors in the NCMRWF unified model (NCUM), Clim. Dyn., 52, 4995–5012, https://doi.org/10.1007/s00382-018-4428-4, 2019.

Katzenberger, A., Schewe, J., Pongratz, J., and Levermann, A.: Robust increase of Indian monsoon rainfall and its variability under future warming in CMIP6 models, Earth Syst. Dynam., 12, 367–386, https://doi.org/10.5194/esd-12-367-2021, 2021.

Keane, R. J., Williams, K. D., Stirling, A. J., Martin, G. M., Birch, C. E., and Parker, D. J.: Fast Biases in Monsoon Rainfall
485   over Southern and Central India in the Met Office Unified Model, Journal of Climate, 32(19), 6385-6402, https://doi.org/10.1175/JCLI-D-18-0650.1, 2019.

Keane, R. J., Parker, D. J., and Fletcher, J. K.: Biases in Indian summer monsoon precipitation forecasts in the Unified Model and their relationship with BSISO index, Geophysical Research Letters, 48, e2020GL090529, https://doi.org/10.1029/2020GL090529, 2021.

490 Kikuchi, K.: Extension of the bimodal intraseasonal oscillation index using JRA-55 reanalysis, Clim. Dyn., 54, 919–933, https://doi.org/10.1007/s00382-019-05037-z, 2020.

Kikuchi, K.: The Boreal Summer Intraseasonal Oscillation (BSISO): A Review, Journal of the Meteorological Society of Japan. Ser. II, 99, 933-972, https://doi.org/10.2151/jmsj.2021-045, 2021.

Kikuchi, K., Wang, B., and Kajikawa, Y.: Bimodal representation of the tropical intraseasonal oscillation, Clim. Dyn., 38,
495 1989–2000, https://doi.org/10.1007/s00382-011-1159-1, 2012.

Kolusu, S. R., Mittermaier, M., Robbins, J., Ashrit, R., and Mitra, A. K.: Novel evaluation of sub-seasonal precipitation ensemble forecasts for identifying high-impact weather events associated with the Indian monsoon, Meteorological Applications, 30(4), e2139, https://doi.org/10.1002/met.2139, 2023.

Lee, J.-Y., Wang, B., Wheeler, M.C., Fu, X., Waliser, D. E., and Kang, I.-S.: Real-time multivariate indices for the boreal
500 summer intraseasonal oscillation over the Asian summer monsoon region, Clim. Dyn. 40, 493–509 https://doi.org/10.1007/s00382-012-1544-4, 2013.

Lee, S.-S., Wang, B., Waliser, D. E., Mani, N. J., and Lee, J.-Y.: Predictability and prediction skill of the boreal summer intraseasonal oscillation in the Intraseasonal Variability Hindcast Experiment, Clim. Dyn., 45, 2123–2135, https://doi.org/10.1007/s00382-014-2461-5, 2015.

505 Levine, R. C. and Turner, A. G.: Dependence of Indian monsoon rainfall on moisture fluxes across the Arabian Sea and the impact of coupled model sea surface temperature biases, Clim. Dyn., 38, 2167–2190, https://doi.org/10.1007/s00382-011-1096-z, 2012.

MacLachlan, C., Arribas, A., Peterson, K. A., Maidens, A., Fereday, D., Scaife, A. A., Gordon, M., Vellinga, M., Williams, A., Comer, R. E., Camp, J., Xavier, P., and Madec, G.: Global Seasonal forecast system version 5 (GloSea5): a high-
510 resolution seasonal forecast system, Q.J.R. Meteorol. Soc., 141, 1072-1084, https://doi.org/10.1002/qj.2396, 2015.

Martin, G. M., Milton, S. F., Senior, C. A., Brooks, M. E., Ineson, S., Reichler, T., and Kim, J.: Analysis and Reduction of Systematic Errors through a Seamless Approach to Modeling Weather and Climate. J. Climate, 23, 5933–5957, https://doi.org/10.1175/2010JCLI3541.1, 2010.

Martin, G. M. and Levine, R. C.: The influence of dynamic vegetation on the present-day simulation and future projections of
515 the South Asian summer monsoon in the HadGEM2 family, Earth Syst. Dynam., 3, 245–261, https://doi.org/10.5194/esd-3-245-2012, 2012.

Martin, G. M., Levine, R. C., Rodriguez, J. M., and Vellinga, M.: Understanding the development of systematic errors in the Asian summer monsoon, Geosci. Model Dev., 14, 1007–1035, https://doi.org/10.5194/gmd-14-1007-2021, 2021.

Menon, A., Turner, A. G., Martin, G. M., and MacLachlan, C.: Modelling the moistening of the free troposphere during the northwestward progression of Indian monsoon onset. Q. J. R. Meteorol. Soc., 144, 1152– 1168, https://doi.org/10.1002/qj.3281, 2018.

Mitra, A.: A Comparative Study on the Skill of CMIP6 Models to Preserve Daily Spatial Patterns of Monsoon Rainfall Over India, Front. Clim., 3, 654763, 10.3389/fclim.2021.654763, 2021.

Pradhan, M., Rao, A. S., Srivastava, A., Dakate, A., Salunke, K., and Shameera, K. S.: Prediction of Indian Summer-Monsoon Onset Variability: A Season in Advance, Scientific Reports, 7(1), 1-14, https://doi.org/10.1038/s41598-017-12594-y, 2017.

Ramu, D. A., Sabeerali, C. T., Chattopadhyay, R., Rao, D. N., George, G., Dhakate, A. R., Salunke, K., Srivastava, A., and Rao, S. A.: Indian summer monsoon rainfall simulation and prediction skill in the CFSv2 coupled model: Impact of atmospheric horizontal resolution, J. Geophys. Res. Atmos., 121, 2205– 2221, doi:10.1002/2015JD024629, 2016.

Rao, S. A., Goswami, B.N., Sahai, A.K., Rajagopal, E.N., Mukhopadhyay, P., Rajeevan, M., Nayak, S., Rathore, L.S., Shenoi, S.S.C., Ramesh, K.J., Nanjundiah, R.S., Ravichandran, M., Mitra, A.K., Pai, D.S., Bhowmik, S.K.R., Hazra, A., Mahapatra, S., Saha, S.K., Chaudhari, H.S., Joseph, S., Sreenivas, P., Pokhrel, S., Pillai, P.A., Chattopadhyay, R., Deshpande, M., Krishna, R.P.M., Das, R.S., Prasad, V.S., Abhilash, S., Panickal, S., Krishnan, R., Kumar, S., Ramu, D.A., Reddy, S.S., Arora, A., Goswami, T., Rai, A., Srivastava, A., Pradhan, M., Tirkey, S., Ganai, M., Mandal, R., Dey, A., Sarkar, S., Malviya, S., Dhakate, A., Salunke, K., and Maini, P.: Monsoon Mission: A Targeted Activity to Improve Monsoon Prediction across Scales. Bull. Amer. Meteor. Soc., 100, 2509–2532, https://doi.org/10.1175/BAMS-D-17-0330.1, 2019.

Ridley, J. K., Blockley, E. W., Keen, A. B., Rae, J. G. L., West, A. E., and Schroeder, D.: The sea ice model component of HadGEM3-GC3.1, Geosci. Model Dev., 11, 713–723, https://doi.org/10.5194/gmd-11-713-2018, 2018.

Rodríguez, J. M. and Milton, S. F.: East Asian Summer Atmospheric Moisture Transport and Its Response to Interannual Variability of the West Pacific Subtropical High: An Evaluation of the Met Office Unified Model, Atmosphere, 10, 457, https://doi.org/10.3390/atmos10080457, 2019.

Rodwell, M.J. and Palmer, T.N. : Using numerical weather prediction to assess climate models, Q.J.R. Meteorol. Soc., 133, 129-146. https://doi.org/10.1002/qj.23, 2007.

Sabeerali, C. T., Dandi, A. R., Dhakate, A., Salunke, K., Mahapatra, S., and Rao, S. A.: Simulation of boreal summer intraseasonal oscillations in the latest CMIP5 coupled GCMs, Journal of Geophysical Research: Atmospheres, 118(10), 4401-4420, https://doi.org/10.1002/jgrd.50403, 2013.

Saha, S., Moorthi, S., Wu, X., Wang, J., Nadiga, S., Tripp, P., Behringer, D., Hou, Y., Chuang, H., Iredell, M., Ek, M., Meng, J., Yang, R., Mendez, M., van den Dool, H., Zhang, Q., Wang, W., Chen, M., and Becker, E.: The NCEP Climate Forecast System Version 2, Journal of Climate, 27(6), 2185-2208, https://doi.org/10.1175/JCLI-D-12-00823.1, 2014.

Sahana, A. S., Pathak, A., Roxy, M. K., and Ghosh, S.: Understanding the role of moisture transport on the dry bias in indian monsoon simulations by CFSv2, Clim. Dyn., 52, 637–651, https://doi.org/10.1007/s00382-018-4154-y, 2019.

Srivastava, A., Rao, S. A., Nagarjuna Rao, D., George, G., and Pradhan, M.: Structure, characteristics, and simulation of monsoon low-pressure systems in CFSv2 coupled model, J. Geophys. Res. Oceans, 122, 6394–6415, doi:10.1002/2016JC012322, 2017.

Srivastava, A., Rao, S. A., and Ghosh, S. Improving the subseasonal variability of the Indian summer monsoon in a climate
555   model, International Journal of Climatology, 43(11), 5227–5247, https://doi.org/10.1002/joc.8142, 2023.

Storkey, D., Blaker, A. T., Mathiot, P., Megann, A., Aksenov, Y., Blockley, E. W., Calvert, D., Graham, T., Hewitt, H. T., Hyder, P., Kuhlbrodt, T., Rae, J. G. L., and Sinha, B.: UK Global Ocean GO6 and GO7: a traceable hierarchy of model resolutions, Geosci. Model Dev., 11, 3187–3213, https://doi.org/10.5194/gmd-11-3187-2018, 2018.

Swapna, P., Krishnan, R., Sandeep, N., Prajeesh, A. G., Ayantika, D. C., Manmeet, S., and Vellore, R.: Long-term climate
560   simulations using the IITM earth system model (IITM-ESMv2) with focus on the South Asian monsoon, Journal of Advances in Modeling Earth Systems, 10, 1127– 1149, https://doi.org/10.1029/2017MS001262, 2018.

Walters, D., Baran, A. J., Boutle, I., Brooks, M., Earnshaw, P., Edwards, J., Furtado, K., Hill, P., Lock, A., Manners, J., Morcrette, C., Mulcahy, J., Sanchez, C., Smith, C., Stratton, R., Tennant, W., Tomassini, L., Van Weverberg, K., Vosper, S., Willett, M., Browse, J., Bushell, A., Carslaw, K., Dalvi, M., Essery, R., Gedney, N., Hardiman, S., Johnson, B., Johnson,
565   C., Jones, A., Jones, C., Mann, G., Milton, S., Rumbold, H., Sellar, A., Ujiie, M., Whitall, M., Williams, K., and Zerroukat, M.: The Met Office Unified Model Global Atmosphere 7.0/7.1 and JULES Global Land 7.0 configurations, Geosci. Model Dev., 12, 1909–1963, https://doi.org/10.5194/gmd-12-1909-2019, 2019.

Wang, B., and Xie, X.: A Model for the Boreal Summer Intraseasonal Oscillation, J. Atmos. Sci., 54, 72–86, https://doi.org/10.1175/1520-0469(1997)054<0072:AMFTBS>2.0.CO;2, 1997.

570   Watterson, I. G., Keane, R. J., Dix, M., Ziehn, T., Andrews, T., Tang, Y.: Analysis of CMIP6 atmospheric moisture fluxes and the implications for projections of future change in mean and heavy rainfall, Int. J. Climatol., 41 (S1), E1417– E1434, https://doi.org/10.1002/joc.6777, 2021.

Williams, K. D., Harris, C. M., Bodas-Salcedo, A., Camp, J., Comer, R. E., Copsey, D., Fereday, D., Graham, T., Hill, R., Hinton, T., Hyder, P., Ineson, S., Masato, G., Milton, S. F., Roberts, M. J., Rowell, D. P., Sanchez, C., Shelly, A., Sinha,
575   B., Walters, D. N., West, A., Woollings, T., and Xavier, P. K.: The Met Office Global Coupled model 2.0 (GC2) configuration, Geosci. Model Dev., 8, 1509–1524, https://doi.org/10.5194/gmd-8-1509-2015, 2015.

Williams, K. D., Copsey, D., Blockley, E. W., Bodas-Salcedo, A., Calvert, D., Comer, R., Davis, P., Graham, T., Hewitt, H. T., Hill, R., Hyder, P., Ineson, S., Johns, T. C., Keen, A. B., Lee, R. W., Megann, A., Milton, S. F., Rae, J. G. L., Roberts, M. J., Scaife, A. A., Schiemann, R., Storkey, D., Thorpe, L., Watterson, I. G., Walters, D. N., West, A., Wood, R. A.,
580   Woollings, T., and Xavier, P. K.: The Met Office Global Coupled Model 3.0 and 3.1 (GC3.0 and GC3.1) Configurations, J. Adv. Model. Earth Sy., 10, 357–380, https://doi.org/10.1002/2017MS001115, 2018.